Acta Mech 225, 1699–1733 (2014)
DOI 10.1007/s00707-013-0998-8

Mohammad Rezaiee-Pajand · Ferdinando Auricchio · Mehrzad Sharifian · Mehrdad Sharifian

Computational plasticity of mixed hardening pressure-dependency constitutive equations

Received: 14 February 2013 / Published online: 12 November 2013

Abstract In the present study, two semi-implicit schemes, based on the exponential maps method, are derived for integrating the pressure-sensitive constitutive equations. In spite of the fact that the consistent tangent operator is necessary to preserve the quadratic rate for the asymptotic convergence of the Newton-Raphson solution in the finite element analyses, there exists no derivation of this operator for the exponential-based integrations of the pressure-sensitive plasticity in the literature. To fulfill this need, the algorithmic tangent operators are extracted for the new semi-implicit as well as the former exponential-based integrations. Moreover, for the accurate integration presented by Rezaiee-Pajand et al. (Eur J Mech A Solids 30:345–361, 2011), the consistent tangent operator is obtained. Eventually, all the investigations are assessed by a broad range of numerical tests.

1 Introduction

In the nonlinear elastoplastic finite element analysis, updating stress is an important and delicate problem which is carried out by integrating the constitutive equations at each Gauss point. It is worth pointing out that the accuracy and efficiency of the aforementioned integration directly affect the final results of the finite element solution. Due to the importance of the issue, study and research in this area have been initiated a long time ago and will be continued in the future. The first investigation was performed by Wilkins [1] presenting the well-known radial return algorithm. Succeeding that, Krieg and Krieg [2], first of all, derived an exact solution for the perfect plasticity defining an angle between the stress and strain rate in the deviatoric plane. In their comprehensive study, iso-error maps were originally proposed as a strong tool to meticulously examine the accuracy of the numerical integrations. On the other hand, an algorithmic tangent operator is required to obtain the structure stiffness matrix for use in the implicit finite element codes. Consistency between the integration scheme and the tangent operator preserves the quadratic convergence rate in the solution of the nonlinear finite element algebraic equations based on Newton's iterative procedure. This issue was first identified by Nagtegaal [3] and followed by Simo and Taylor [4] and Dodds [5]. It should be noted that investigation on the stability of the integration methods in plasticity was initially performed by Ortiz and Popov [6]. In the case of the plane stress problem, the integration method will not be a minor modification of three-dimensional integration the

M. Rezaiee-Pajand (✉)
Department of Civil Engineering, Ferdowsi University of Mashhad, Mashhad, Iran
E-mail: mrpajand@yahoo.com

F. Auricchio
Department of Civil Engineering and Architecture, University of Pavia, Pavia, Italy

M. Sharifian · M. Sharifian
Department of Structural Engineering, Ferdowsi University of Mashhad, Mashhad, Iran

way the plane strain problem is. Simo and Taylor [7] are perceived as the pioneers to suggest a return mapping technique for the plane stress conditions.

The numerical techniques in computational plasticity are being developed along with extending the constitutive equations to more realistically simulate the material behavior. In the following lines, some of the advances are briefly reviewed. It is convenient that the integration methods be classified into two general groups of explicit and implicit techniques.

In the explicit methods, the stress state and internal variables are updated based on the known quantities at the beginning of the load step, and there is no iterative process in the main part of the solution. The explicit integration procedures could be divided into three categories. One group comprises the methods that directly integrate the constitutive equations via an explicit Runge–Kutta (RK) technique, such as Forward Euler, modified Euler, Heun's RK method, fourth-order RK methods. In this case, the final stress must be corrected by placing it on the yield surface because the consistency condition is not automatically held during the stress updating process. Of the many efforts in this area, for example, the researches of Sloan and Booker [8], Potts and Ganendra [9], Sloan et al. [10], Solowski and Gallipoli [11] could be mentioned. In another category, the constitutive equations are reduced to fewer ordinary differential equations (ODEs) by defining angles between plasticity variables. These techniques are usually consistent and use the explicit Runge-Kutta method for solving the ODEs. Studies carried out by Krieg and Krieg [2], Loret and Prevost [12], Ristinmaa and Tryding [13], Wie et al. [14], Wallin and Ristinmaa [15,16], Szabó [17], Kossa and Szabó [18], Rezaiee-Pajand and Sharifian [19] are in the aforementioned category. The third type is exponential-based integrations, which were first introduced by Auricchio and Beirão da Veiga [20] motivated by the researches of Hong and Liu [21,22]. In the latter form, the constitutive equations are converted to the equivalent system of differential equations in the augmented stress space as $\dot{\mathbf{X}} = \mathbb{A}\mathbf{X}$. This equation has a closed-form exponential solution when the matrix $\mathbb{A}$ is constant. Regarding the exponential-based integrations, many investigations could be addressed, such as the works by Liu [23], Artioli et al. [24–26], Rezaiee-Pajand and Nasirai [27,28], Rezaiee-Pajand et al. [29–31]. It is worth mentioning that, although there are some semi-implicit exponential schemes such as works of Rezaiee-Pajand and Nasirai [27,28], the process of the solution, in effect, is explicit and for that reason they need to be classified in the group of explicit integrations.

On the other side, there are implicit integrations where the variables are updated using the unknown states of stress, and as a result, the integration process usually involves an iterative solution. Moreover, the consistency condition is automatically fulfilled. In this area, lots of researches have been carried out thus far, of which the most noticeable are the studies presented by Ortiz and Simo [32], Genna and Pandolfi [33], Hopperstad and Remseth [34], Kobayashi and Ohno [35], Kobayashi et al. [36], Kang [37], Clausen et al. [38], Kan et al. [39] and Coombs et al. [40].

Up to this date, two fully explicit exponential-based integrations have been presented for the mixed hardening Drucker–Prager's constitutive equations, which are a widely used plasticity model to predict the elastoplastic behavior of a broad range of geotechnical materials such as rock, soil, concrete as well as iron-based substances, including aluminum and porous metals. In the present study, it is desired to improve the integration schemes by converting them into semi-implicit strategies, in Sects. 3.3 and 4.3. Moreover, to preserve the quadratic convergence rate in implicit finite element codes, it is necessary that the algorithmic tangent operators of the integrating tactics be derived due to their absence in computational plasticity references, see Sects. 3.2, 3.4, 4.2 and 4.4. The consistent tangent operator for the accurate integration method presented by Rezaiee-Pajand et al. [30] is formulated as well, Sect. 5.2. Finally, to assess the proposed semi-implicit integrations and the consistent tangent operators, a wide range of numerical tests is carried out consisting of strain load histories, iso-error maps and boundary value problems. The numerical investigations clearly demonstrate the merits of the authors' formulations.

2 Basic equations

In what follows, an associative Drucker–Prager's elastoplasticity along with linear isotropic and kinematic hardenings is considered as the constitutive equations. Pursuing standard methodology in plasticity for presenting the basic equations, one can write the following relationships:

$$\boldsymbol{\varepsilon} = \boldsymbol{\varepsilon}^{\mathrm{e}} + \boldsymbol{\varepsilon}^{\mathrm{p}}, \tag{1}$$

$$\boldsymbol{\sigma} = \mathbb{D}^{\mathrm{e}}\boldsymbol{\varepsilon}^{\mathrm{e}}, \tag{2}$$

$$F = \frac{1}{2}\mathbf{s}'^{\mathrm{T}}\mathbf{s}' - (\tau_{\mathrm{y}} - \beta p')^2 = 0, \quad \tau_{\mathrm{y}} - \beta p' > 0, \tag{3}$$

$$\dot{\boldsymbol{\varepsilon}}^{\mathrm{p}} = \dot{\gamma}\frac{\partial F}{\partial \boldsymbol{\sigma}'}, \tag{4}$$

$$\tau_{\mathrm{y}} = \tau_{\mathrm{y0}} + H_{\mathrm{iso}}\gamma, \tag{5}$$

$$\dot{\mathbf{a}} = H_{\mathrm{kin}}\dot{\boldsymbol{\varepsilon}}^{\mathrm{p}}, \tag{6}$$

$$\dot{\gamma} \geq 0, \quad F \leq 0, \quad \dot{\gamma}F = 0. \tag{7}$$

Equation (1) determines the additive decomposition of the strain vector, as $\boldsymbol{\varepsilon}$, $\boldsymbol{\varepsilon}^{\mathrm{e}}$, and $\boldsymbol{\varepsilon}^{\mathrm{p}}$ denote the total strain and its elastic and plastic parts, respectively. The elastic law is represented by Eq. (2), which is the relation between the total stress, $\boldsymbol{\sigma}$, and the elastic strain, $\boldsymbol{\varepsilon}^{\mathrm{e}}$. In this equation, $\mathbb{D}^{\mathrm{e}}$ specifies the standard isotropy elastic stiffness matrix of the material. Equation (3) represents the Drucker–Prager's yield surface [41], in which the yielding of the material is pressure sensitive. Note that this yield criterion is a smooth approximate function of the Mohr-Coulomb plasticity model. The parameters τ_{y} and β are the yield stress in pure shear and a constant of the material. Furthermore, $\mathbf{s}'$ and p' denote the deviatoric and volumetric parts of the shifted stress, $\boldsymbol{\sigma}'$, defined as $\boldsymbol{\sigma}' := \mathbf{s}' + p'\mathbf{i}$ with $p' = 1/3\,\mathrm{tr}(\boldsymbol{\sigma}')$, where $\mathbf{i}$ and $\mathrm{tr}(\cdot)$ are the vector associated with the second-order identity tensor and the trace operator, respectively. The evolution of the plastic part of the strain is defined by an associative flow rule in Eq. (4), where $\dot{\gamma}$ specifies the plastic multiplier. Adopting the linear isotropic hardening law in Eq. (5), the evolution of the yield stress is taken into account during the plastic phase. In this equation, τ_{y0} and H_{iso} are the initial yield stress and the isotropic hardening modulus. To include the Bauschinger effect, a linear kinematic hardening is given in Eq. (6), where $\mathbf{a}$ and H_{kin} designate the back stress and kinematic hardening modulus. It should be noted that the shifted stress, $\boldsymbol{\sigma}'$, is defined as $\boldsymbol{\sigma}' := \boldsymbol{\sigma} - \mathbf{a}$. Finally, the elastoplastic constitutive model is completed having employed the Kuhn-Tucker complimentary conditions in Eq. (7). To present the formulations of the integration algorithms, the following decompositions are introduced:

$$\begin{aligned}
&\boldsymbol{\sigma} = \mathbf{s} + p\mathbf{i}, \qquad p = \frac{1}{3}\mathrm{tr}(\boldsymbol{\sigma}),\\
&\mathbf{a} = \boldsymbol{\alpha} + \bar{p}\mathbf{i}, \qquad \bar{p} = \frac{1}{3}\mathrm{tr}(\mathbf{a}),\\
&\boldsymbol{\varepsilon} = \mathbf{e} + \frac{1}{3}\varepsilon_{\mathrm{v}}^{\mathbf{i}}, \quad \varepsilon_{\mathrm{v}} = \mathrm{tr}(\boldsymbol{\varepsilon}).
\end{aligned} \tag{8}$$

In order to determine the plastic multiplier, the consistency condition is utilized during the plastic behavior of the material, i.e. $\dot{F} = 0$. As a result, one can reach the following equation:

$$\dot{\gamma} = \frac{2G\mathbf{s}'^{\mathrm{T}}\dot{\mathbf{e}} + \sqrt{2}\beta K R\dot{\varepsilon}_{\mathrm{v}}}{2(\bar{G} + \bar{K}\beta^2)R^2 + \sqrt{2}H_{\mathrm{iso}}R}. \tag{9}$$

In this expression, the term R is defined as the radius of the yield surface in the deviatoric plane, and it has the form:

$$R := \sqrt{2}(\tau_{\mathrm{y}} - \beta p'). \tag{10}$$

The constants $\bar{G}$ and $\bar{K}$ have the following definitions:

$$\begin{aligned}
\bar{G} &= G + 1/2H_{\mathrm{kin}},\\
\bar{K} &= K + 1/3H_{\mathrm{kin}},
\end{aligned} \tag{11}$$

where G and K are, respectively, the shear and bulk modulus. Finally, the continuum elastoplastic tangent matrix, which characterizes the relation between the rates of the stress and strain in the elastoplastic phase, can be represented by:

$$\mathbb{D}^{\mathrm{ep}} = \mathbb{D}^{\mathrm{e}} - \frac{(\mathbb{D}^{\mathrm{e}}\partial F/\partial\boldsymbol{\sigma}')(\mathbb{D}^{\mathrm{e}}\partial F/\partial\boldsymbol{\sigma}')^{\mathrm{T}}}{(\partial F/\partial\boldsymbol{\sigma})^{\mathrm{T}}(\mathbb{D}^{\mathrm{e}}\partial F/\partial\boldsymbol{\sigma}') - H_{\mathrm{kin}}(\partial F/\partial\mathbf{a})^{\mathrm{T}}(\mathbb{D}^{\mathrm{e}}\partial F/\partial\boldsymbol{\sigma}') + H_{\mathrm{iso}}(\partial F/\partial\tau_{\mathrm{y}})}. \tag{12}$$

Having obtained the derivatives appearing in the last equation and after some manipulations, the following equation can be expressed as the applicable closed-form continuum elastoplastic tangent matrix:

$$\mathbb{D}^{\mathrm{ep}} = \mathbb{D}^{\mathrm{e}} - \frac{(2G\mathbf{s}' + \sqrt{2}K\beta R\mathbf{i})(2G\mathbf{s}' + \sqrt{2}K\beta R\mathbf{i})^{\mathrm{T}}}{2(\bar{G} + \bar{K}\beta^2)R^2 + \sqrt{2}H_{\mathrm{iso}}\mathbf{R}}. \tag{13}$$

In the following sections, the algorithms of the exponential-based integrations are briefly presented; more details on the formulations can be found in Reference [30]. After presenting the integration algorithms, the corresponding consistent tangent matrixes are derived. Then, two semi-implicit exponential-based integrations are proposed together with their algorithmic tangent operators. Finally, the consistent tangent operator of the accurate integration presented by Rezaiee-Pajand et al. [30] is derived.

3 Exponential-based method with one integrating factor

The original constitutive equations in the exponential-based method using one integrating factor are converted into the following equivalent system of differential equations:

$$\dot{\mathbf{X}} = \mathbb{A}\mathbf{X}, \tag{14}$$

where $\mathbf{X}$ and $\mathbb{A}$ denote the augmented stress vector and the control matrix, respectively, which are defined as

$$\mathbf{X} = \begin{Bmatrix} \mathbf{X}^{\mathrm{s}} \\ X^{\mathrm{R}} \\ X^{0} \end{Bmatrix} = \begin{Bmatrix} X^{0}\mathbf{s}' \\ X^{0}R \\ X^{0} \end{Bmatrix}; \quad \mathbb{A} = \begin{bmatrix} \mathbb{O}_{9\times 9} & \frac{2G}{R}\dot{\mathbf{e}} & \mathbf{0}_{9\times 1} \\ \frac{2G}{R}\dot{\mathbf{e}}^{\mathrm{T}} & 0 & 0 \\ \frac{2G}{Q}\dot{\mathbf{e}}^{\mathrm{T}} & \frac{\sqrt{2}\beta K}{Q}\dot{\varepsilon}_{\mathrm{v}} & 0 \end{bmatrix}_{11\times 11}. \tag{15}$$

In the above expressions, $\mathbf{0}_{9\times 1}$ and $\mathbb{O}_{9\times 9}$ specify the null vector and matrix, respectively. The parameter X^0 denotes the integrating factor. Furthermore, the scalar parameter Q and the integrating factor X^0, appearing in the matrix $\mathbb{A}$, have the following form:

$$Q = \frac{\sqrt{2}(\bar{G} + \bar{K}\beta^2)R^2 + H_{\mathrm{iso}}R}{\sqrt{2}\bar{G}}, \tag{16}$$

$$X^0 = \exp(2\bar{G}\gamma). \tag{17}$$

In the rest of this section, in order to derive the consistent tangent operator of the fully explicit exponential-based integration with one integrating factor, firstly, the integration algorithm is concisely reviewed. Then, a semi-implicit integration and its consistent tangent operator are developed.

3.1 Explicit integration algorithm with one factor (explicit-I)

The fully explicit integration with one factor was previously developed in [30]. Here, it is briefly presented for deriving its consistent tangent operator in the next section. Following the standard methodology, a generic time step (*pseudo time* step) from t_n to t_{n+1} is considered as the material state $\{\mathbf{a}_n,\ \boldsymbol{\sigma}_n,\ \gamma_n,\ \boldsymbol{\varepsilon}^{\mathrm{p}}_n\}$ at time t_n, and the strain path is known. The algorithm should characterize the stress and interval variables at time t_{n+1}. Like with all explicit integrations, first, the next tentative solution is used:

$$\begin{aligned} \mathbf{s}'^{\mathrm{TR}}_{n+1} &= \mathbf{s}'_n + 2G\Delta\mathbf{e} \quad \text{and} \quad p'^{\mathrm{TR}}_{n+1} = p'_n + K\Delta\varepsilon_{\mathrm{v}}, \\ \boldsymbol{\alpha}^{\mathrm{TR}}_{n+1} &= \boldsymbol{\alpha}_n \qquad\qquad \text{and} \quad \bar{p}^{\mathrm{TR}}_{n+1} = \bar{p}_n, \\ \tau^{\mathrm{TR}}_{\mathrm{y},n+1} &= \tau_{\mathrm{y},n}. \end{aligned} \tag{18}$$

Afterward, one must check the trial elastic solution through the following condition:

$$\left\|\mathbf{s}'^{\mathrm{TR}}_{n+1}\right\|^2 \le 2\left(\tau^{\mathrm{TR}}_{\mathrm{y},n+1} - \beta p'^{\mathrm{TR}}_{n+1}\right)^2. \tag{19}$$

If the condition is met, the trial solution is the final one. Otherwise, the time step is partly elastic and partly elastoplastic. These portions can be separated by introducing a scalar parameter $0 \le \alpha < 1$ as $\alpha\Delta t$ and $(1-\alpha)\Delta t$ to specify the elastic and elastoplastic parts. How to compute the parameter α is shown in Appendix A. Having the scalar parameter α in hand, the stress state at the contact point with the yield surface is readily found using the elastic law:

$$\begin{aligned} \mathbf{s}'_{n+\alpha} &= \mathbf{s}'_n + 2G\alpha\Delta\mathbf{e}, \\ p'_{n+\alpha} &= p'_n + K\alpha\Delta\varepsilon_{\mathrm{v}}. \end{aligned} \tag{20}$$

The computations are followed by integrating the set of the differential equations (14) in the elastoplastic phase. There is a closed-form solution to the differential system as long as the multiplier matrix $\mathbb{A}$ has constant coefficients. However, the matrix $\mathbb{A}$ is not constant owing to the parameter R varying in it. Therefore, it is approximately assumed that the value of the yield surface radius is equal to its value at the end of the elastic part of the time step, i.e., at the contact point. Based on this explanation, the dynamical system can exactly be solved as follows:

$$\mathbf{X}_{n+1} = \exp[\mathbb{A}_{n+\alpha}(1-\alpha)\Delta t]\mathbf{X}_{n+\alpha} = \mathbb{G}_{n+\alpha}\mathbf{X}_{n+\alpha}, \tag{21}$$

$$\mathbb{G}_{n+\alpha} = \begin{bmatrix} \mathbb{I}_{9\times 9} + (a_{n+\alpha}-1)\Delta\hat{\mathbf{e}}\Delta\hat{\mathbf{e}}^{\mathrm{T}} & b_{n+\alpha}\Delta\hat{\mathbf{e}} & \mathbf{0}_{9\times 1} \\ b_{n+\alpha}\Delta\hat{\mathbf{e}}^{\mathrm{T}} & a_{n+\alpha} & 0 \\ [c_{n+\alpha}b_{n+\alpha} + (a_{n+\alpha}-1)d_{n+\alpha}]\Delta\hat{\mathbf{e}}^{\mathrm{T}} & d_{n+\alpha}b_{n+\alpha} + (a_{n+\alpha}-1)c_{n+\alpha} & 1 \end{bmatrix}_{11\times 11}. \tag{22}$$

For computing the matrix exponential, one could find the reference [42] useful. In the last relationship, $\mathbb{I}$ and $\Delta\hat{\mathbf{e}}$ represent, respectively, the identity matrix and the unit vector of the deviatoric strain increment. Besides, the scalar parameters in matrix $\mathbb{G}_{n+\alpha}$ are given as follows:

$$\begin{aligned} a_{n+\alpha} &= \cosh\left[(1-\alpha)\frac{2G}{R_{n+\alpha}}\|\Delta\mathbf{e}\|\right], \quad b_{n+\alpha} = \sinh\left[(1-\alpha)\frac{2G}{R_{n+\alpha}}\|\Delta\mathbf{e}\|\right], \\ c_{n+\alpha} &= \frac{R_{n+\alpha}}{Q_{n+\alpha}}, \quad d_n = \frac{\beta K R_{n+\alpha}}{\sqrt{2}GQ_{n+\alpha}}\frac{\Delta\varepsilon_{\mathrm{v}}}{\|\Delta\mathbf{e}\|}. \end{aligned} \tag{23}$$

Now, having the vector $\mathbf{X}_{n+1}$ computed by Eq. (21), the deviatoric shifted stress and the radius of the yield surface at time t_{n+1} are immediately acquired using the following equations:

$$\mathbf{s}'_{n+1} = \frac{\mathbf{X}^{\mathrm{s}}_{n+1}}{X^0_{n+1}}, \tag{24}$$

$$R_{n+1} = \frac{X^{\mathrm{R}}_{n+1}}{X^0_{n+1}}. \tag{25}$$

To update the yield stress, τ_{y}, it is required that the discrete plastic multiplier ($\lambda = \gamma_{n+1} - \gamma_n$) be determined by directly utilizing Eq. (17), in this manner:

$$\lambda = \frac{1}{2\bar{G}}\ln\left(\frac{X^0_{n+1}}{X^0_n}\right). \tag{26}$$

Therefore, the yield stress can easily be expressed as:

$$\tau_{\mathrm{y},n+1} = \tau_{\mathrm{y},n} + \lambda H_{\mathrm{iso}}. \tag{27}$$

Then, based on Eq. (6), the back stress can be updated in the following form:

$$\boldsymbol{\alpha}_{n+1} = \boldsymbol{\alpha}_n + H_{\mathrm{kin}}\Delta\mathbf{e}^{\mathrm{p}}. \tag{28}$$

The increment of the deviatoric plastic strain is achieved as $\Delta\mathbf{e}^{\mathrm{p}} = 1/2\bar{G}(\mathbf{s}'^{\mathrm{TR}}_{n+1} - \mathbf{s}'_{n+1})$. Finally, the hydrostatic pressure can be determined by:

$$p_{n+1} = p_n + K\Delta\varepsilon_{\mathrm{v}} - \sqrt{2}\beta K\left\|\Delta\mathbf{e}^{\mathrm{p}}\right\|. \tag{29}$$

It should be mentioned that as soon as the volumetric part of the shifted stress at time t_{n+1} computed by the definition of the yield surface radius, the volumetric part of the back stress, $\bar{p}_{n+1}$, is easily attained subtracting p'_{n+1} from p_{n+1}. In addition, the integrating factor X^0 is a local auxiliary variable which may be equal to 1 at the beginning of each time step. Treatment of the apex, also, has been completely presented in Reference [30].

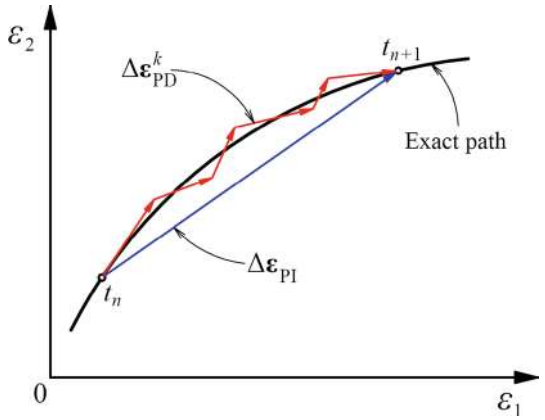

Fig. 1 Different strategies for determining strain path [5]

3.2 Consistent tangent operator for explicit-I scheme

Using an implicit manner in the elastoplastic finite element analysis, an iterative Newton-Raphson solution is commonly used for solving the nonlinear algebraic equations in each generic load increment from t_n to t_{n+1}. In this kind of analysis, the path-independent strategy has been utilized if the constitutive equations are integrated over the total strain increment, i.e., $\Delta\boldsymbol{\varepsilon}^k_{\mathrm{PI}} = \boldsymbol{\varepsilon}^k_{n+1} - \boldsymbol{\varepsilon}_n$, using the initial conditions on the basis of the converged results at time $t = t_n$ in each Newton's iteration (denoted by k). In other words, at every iteration of a load increment, the initial conditions for computing the material states are the same and equal to the values at the beginning of the load increment. As a result, the obtained strain path will be a linear portion as illustrated in Fig. 1. On the other hand, the path-dependent strategy will be applied in finding the strain path for updating stress and internal variables if the constitutive equations are integrated over the iterative increment of strain, i.e. $\Delta\boldsymbol{\varepsilon}^k_{\mathrm{PD}} = \boldsymbol{\varepsilon}^k_{n+1} - \boldsymbol{\varepsilon}^{k-1}_{n+1}$, using the initial conditions based on the non-converged results at time t^{k-1}_{n+1}. Consequently, the strain path of each load increment comprises several linear segments.

Using the path-dependent strategy can yield some disadvantages [5]. The direction of the plastic flow may be noticeably different in successive iterations, because of the direction of the strain iterative increments diverting from the real strain path. In fact, the overall effect of these deviations may not properly match with the actual direction of the plastic flow that differs smoothly over the total load increment. Moreover, changing severely the direction of the successive strain increments could result in locating the tentative elastic stress point in the elastic domain, i.e. inside the yield surface, and as a consequence, false elastic unloading would occur. Therefore, it can be seen that the residual norm may be increased during some subsequent iterations, and even the solution may diverge after a few iterations.

Based on the aforementioned explanation, using a path-independent strategy in the elastoplastic finite element analysis is necessary. Additionally, in implicit codes, if the continuum tangent operator is used, the result will be the loss of the quadratic rate of the asymptotic convergence of the Newton method for the global solution. In fact, the predicted stress increment in the kth iteration by the continuum tangent operator will merely match the stress increment achieved by the integration algorithm to first order when the load steps are in the infinitesimal realm. Therefore, for preserving the rapid convergence of the Newton method, it is imperative that the stress updating algorithm be linearized. The linearization of the integration algorithm contributes to a *consistent* (or *algorithmic*) elastoplastic tangent operator.

In order to use the exponential-based algorithm, presented in the previous section, in the implicit finite element codes, the following algorithmic tangent operator is required:

$$\frac{\partial\boldsymbol{\sigma}_{n+1}}{\partial\boldsymbol{\varepsilon}_{n+1}} = \frac{\partial\mathbf{s}_{n+1}}{\partial\boldsymbol{\varepsilon}_{n+1}} + \left(\frac{\partial p_{n+1}}{\partial\boldsymbol{\varepsilon}_{n+1}}\right)^{\mathrm{T}}\mathbf{i}. \tag{30}$$

Since the deviatoric stress, $\mathbf{s}$, is a function of $\mathbf{s}'$ and $\boldsymbol{\alpha}$, the last equation is extended to the next one:

$$\frac{\partial\boldsymbol{\sigma}_{n+1}}{\partial\boldsymbol{\varepsilon}_{n+1}} = \left(\frac{\partial\mathbf{s}'_{n+1}}{\partial\mathbf{e}_{n+1}} + \frac{\partial\boldsymbol{\alpha}_{n+1}}{\partial\mathbf{e}_{n+1}}\right)\mathbb{I}_{\mathrm{dev}} + \left(\frac{\partial p_{n+1}}{\partial\boldsymbol{\varepsilon}_{n+1}}\right)^{\mathrm{T}}\mathbf{i}, \tag{31}$$

where $\mathbb{I}_{\text{dev}} = \mathbb{I} - 1/3\mathbf{i}\mathbf{i}^T$ and the derivatives appeared in the last equation need to be derived. To calculate the term $(\partial \mathbf{s}'/\partial \mathbf{e})_{n+1}$, one should refer to Eq. (24) and take its derivative with respect to $\mathbf{e}_{n+1}$, as follows:

$$\frac{\partial \mathbf{s}'_{n+1}}{\partial \mathbf{e}_{n+1}} = \frac{1}{X^0_{n+1}} \frac{\partial \mathbf{X}^{\text{s}}_{n+1}}{\partial \mathbf{e}_{n+1}} - \frac{\mathbf{X}^{\text{s}}_{n+1}}{(X^0_{n+1})^2} \left(\frac{\partial X^0_{n+1}}{\partial \mathbf{e}_{n+1}} \right)^{\text{T}}. \tag{32}$$

The above equation indicates the expressions for $\mathbf{X}^{\text{s}}_{n+1}$ and X^0_{n+1} that must be drawn by expanding Eq. (21), and after that, taking the derivatives of the results bestows the following relations:

$$\begin{aligned} \frac{\partial \mathbf{X}^{\text{s}}_{n+1}}{\partial \mathbf{e}_{n+1}} = {} & \frac{\partial \mathbf{X}^{\text{s}}_{n+\alpha}}{\partial \mathbf{e}} + \left(\Delta \hat{\mathbf{e}}^T \mathbf{X}^{\text{s}}_{n+\alpha} \right) \Delta \hat{\mathbf{e}} \left(\frac{\partial a}{\partial \mathbf{e}} \right)^{\text{T}} + (a-1) \left(\Delta \hat{\mathbf{e}}^{\text{T}} \mathbf{X}^{\text{s}}_{n+\alpha} \right) \frac{\partial \Delta \hat{\mathbf{e}}}{\partial \mathbf{e}} + (a-1) \Delta \hat{\mathbf{e}} \left(\frac{\partial \Delta \hat{\mathbf{e}}}{\partial \mathbf{e}} \mathbf{X}^{\text{s}}_{n+\alpha} \right)^{\text{T}}, \\ & + (a-1) \Delta \hat{\mathbf{e}} \left(\frac{\partial \mathbf{X}^{\text{s}}_{n+\alpha}}{\partial \mathbf{e}} \Delta \hat{\mathbf{e}} \right)^{\text{T}} + X^{\text{R}}_{n+\alpha} \Delta \hat{\mathbf{e}} \left(\frac{\partial b}{\partial \mathbf{e}} \right) + b X^{\text{R}}_{n+\alpha} \frac{\partial \Delta \hat{\mathbf{e}}}{\partial \mathbf{e}} + b \Delta \hat{\mathbf{e}} \left(\frac{\partial X^{\text{R}}_{n+\alpha}}{\partial \mathbf{e}} \right), \end{aligned} \tag{33}$$

$$\begin{aligned} \frac{\partial X^0_{n+1}}{\partial \mathbf{e}_{n+1}} = {} & \left[b \frac{\partial c}{\partial \mathbf{e}} + c \frac{\partial b}{\partial \mathbf{e}} + (a-1) \frac{\partial d}{\partial \mathbf{e}} + d \frac{\partial a}{\partial \mathbf{e}} \right] \Delta \hat{\mathbf{e}}^{\text{T}} \mathbf{X}^{\text{s}}_{n+\alpha} + [c \cdot b + (a-1)d] \frac{\partial \Delta \hat{\mathbf{e}}}{\partial \mathbf{e}} \mathbf{X}^{\text{s}}_{n+\alpha} \\ & + [c \cdot b + (a-1)d] \frac{\partial \mathbf{X}^{\text{s}}_{n+\alpha}}{\partial \mathbf{e}} \Delta \hat{\mathbf{e}} + \left[d \frac{\partial b}{\partial \mathbf{e}} + b \frac{\partial d}{\partial \mathbf{e}} + (a-1) \frac{\partial c}{\partial \mathbf{e}} + c \frac{\partial a}{\partial \mathbf{e}} \right] X^{\text{R}}_{n+\alpha} \\ & + [d \cdot b + (a-1)c] \frac{\partial X^{\text{R}}_{n+\alpha}}{\partial \mathbf{e}}. \end{aligned} \tag{34}$$

In these equations, all parameters a, b, c and d have subscript $n+\alpha$. The derivatives appearing in Eqs. (33) and (34) will be presented in Appendix B since they require many steps. In order to determine $(\partial \boldsymbol{\alpha}/\partial \mathbf{e})_{n+1}$, the derivative of Eq. (28) is also needed:

$$\frac{\partial \boldsymbol{\alpha}_{n+1}}{\partial \mathbf{e}_{n+1}} = H_{\text{kin}} \frac{\partial \Delta \mathbf{e}^{\text{p}}}{\partial \mathbf{e}_{n+1}}. \tag{35}$$

The term $(\partial \Delta \mathbf{e}^{\text{p}}/\partial \mathbf{e})_{n+1}$ can be found by differentiating the expression $1/2\bar{G}(\mathbf{s}'^{\text{TR}}_{n+1} - \mathbf{s}'_{n+1})$ with respect to $\mathbf{e}_{n+1}$ in the form:

$$\frac{\partial \Delta \mathbf{e}^{\text{p}}}{\partial \mathbf{e}_{n+1}} = \frac{G}{\bar{G}} \mathbb{I} - \frac{1}{2\bar{G}} \frac{\partial \mathbf{s}'_{n+1}}{\partial \mathbf{e}_{n+1}}. \tag{36}$$

Finally, having calculated $(\partial p/\partial \boldsymbol{\varepsilon})_{n+1}$, all the derivatives needed for computing the algorithmic tangent operator will be at hand. This derivative can be specified using Eq. (29) as follows:

$$\frac{\partial p_{n+1}}{\partial \boldsymbol{\varepsilon}_{n+1}} = K \mathbf{i} - \sqrt{2} \beta K \mathbb{I}_{\text{dev}} \frac{\partial \Delta \mathbf{e}^{\text{p}}}{\partial \mathbf{e}_{n+1}} \Delta \hat{\mathbf{e}}^{\text{p}}, \tag{37}$$

where $\Delta \hat{\mathbf{e}}^{\text{p}}$ denotes the unit vector of $\Delta \mathbf{e}^{\text{p}}$, i.e. $\Delta \hat{\mathbf{e}}^{\text{p}} = \Delta \mathbf{e}^{\text{p}} / \| \Delta \mathbf{e}^{\text{p}} \|$.

3.3 Semi-implicit integration algorithm with one factor (semi-implicit-I)

In the present section, it is desired to develop a semi-implicit integration. In fact, the fully explicit scheme, explained in the previous section, could be improved by implementing the semi-implicit technique. This was first proposed by Rezaiee-Pajand and Nasirai [27,28] for the augmented constitutive laws. The main idea of this methodology is to find the variables of the control matrix $\mathbb{A}$ at the middle of the elasoplastic part of the load step rather than considering their values at the beginning. This way, the accuracy increases due to estimating better values for R. To reach the purpose, the value of the yield surface radius is computed at the general specific time $t = t_{n+r(1-\alpha)}$ with $0 < r \leq 1$, where $R_{n+r(1-\alpha)}$ utilizes the result of the following equation:

$$\mathbf{X}_{n+r(1-\alpha)} = \exp[\mathbb{A}_{n+\alpha} r(1-\alpha) \Delta t] \mathbf{X}_{n+\alpha}. \tag{38}$$

At this stage, one could obtain R at the time $t = t_{n+r(1-\alpha)}$ by the last equation as:

$$R_{n+r(1-\alpha)} = \frac{\bar{b}_{n+\alpha}\Delta\hat{\mathbf{e}}^{\mathrm{T}}\mathbf{s}'_{n+\alpha} + \bar{a}_{n+\alpha}R_{n+\alpha}}{[c_{n+\alpha}\bar{b}_{n+\alpha} + (\bar{a}_{n+\alpha}-1)d_{n+\alpha}]\Delta\hat{\mathbf{e}}^{\mathrm{T}}\mathbf{s}'_{n+\alpha} + [d_{n+\alpha}\bar{b}_{n+\alpha} + (\bar{a}_{n+\alpha}-1)c_{n+\alpha}]R_{n+\alpha} + 1}, \tag{39}$$

$$\begin{aligned} \bar{a}_{n+\alpha} &= \cosh\left[\frac{2G}{R_{n+\alpha}}\|r(1-\alpha)\Delta\mathbf{e}\|\right], \\ \bar{b}_{n+\alpha} &= \sinh\left[\frac{2G}{R_{n+\alpha}}\|r(1-\alpha)\Delta\mathbf{e}\|\right]. \end{aligned} \tag{40}$$

Having $R_{n+r(1-\alpha)}$, the augmented vector $\mathbf{X}_{n+1}$ could be calculated by Eq. (21) just with the difference that $R_{n+r(1-\alpha)}$ should be substituted for $R_{n+\alpha}$ as

$$\mathbf{X}_{n+1} = \exp\left[\mathbb{A}_{n+r(1-\alpha)}(1-\alpha)\Delta t\right]\mathbf{X}_{n+\alpha} = \mathbb{G}_{n+r(1-\alpha)}\mathbf{X}_{n+\alpha}, \tag{41}$$

where the matrix $\mathbb{G}_{n+r(1-\alpha)}$ is defined by:

$$\mathbb{G}_{n+r(1-\alpha)} = \begin{bmatrix} \mathbb{I}_{9\times 9} + (a_{n+r(1-\alpha)}-1)\Delta\hat{\mathbf{e}}\Delta\hat{\mathbf{e}}^{\mathrm{T}} & b_{n+r(1-\alpha)}\Delta\hat{\mathbf{e}} & \mathbf{0}_{9\times 1} \\ b_{n+r(1-\alpha)}\Delta\hat{\mathbf{e}}^{\mathrm{T}} & a_{n+r(1-\alpha)} & 0 \\ [c.b + (a-1)d]_{n+r(1-\alpha)}\,\Delta\hat{\mathbf{e}}^{\mathrm{T}} & [d.b + (a-1)c]_{n+r(1-\alpha)} & 1 \end{bmatrix}_{11\times 11}. \tag{42}$$

The parameters a, b, c and d with the subscript of $n + r(1-\alpha)$ are determined from the below relationships:

$$\begin{aligned} a_{n+r(1-\alpha)} &= \cosh\left(\frac{2G}{R_{n+r(1-\alpha)}}\|\Delta\mathbf{e}\|\right), \\ b_{n+r(1-\alpha)} &= \sinh\left(\frac{2G}{R_{n+r(1-\alpha)}}\|\Delta\mathbf{e}\|\right), \\ c_{n+r(1-\alpha)} &= \frac{R_{n+r(1-\alpha)}}{Q_{n+r(1-\alpha)}}, \\ d_{n+r(1-\alpha)} &= \frac{R_{n+r(1-\alpha)}}{Q_{n+r(1-\alpha)}}V. \end{aligned} \tag{43}$$

Once $\mathbf{X}_{n+1}$ is known, the other constitutive parameters are easily computed through Eqs. (24)–(29).

3.4 Consistent tangent operator for semi-implicit-I scheme

Finding the consistent tangent operator is equivalent to determining the derivative terms in Eq. (31), which is the goal of this section. In the case of $(\partial\mathbf{s}'/\partial\mathbf{e})_{n+1}$, the expressions given in Eqs. (32)–(34) could be employed, but since the vector $\mathbf{X}^{\mathrm{s}}_{n+1}$ and scalar X^{0}_{n+1} have different relations here with respect to the explicit scheme, the scalar parameters a, b, c and d have the subscript $n + r(1-\alpha)$. The derivatives of these parameters will be provided in Appendix C. The other terms appearing in Eq. (31), i.e. $(\partial\boldsymbol{\alpha}/\partial\mathbf{e})_{n+1}$ and $(\partial p/\partial\boldsymbol{\varepsilon})_{n+1}$, are achievable via Eqs. (35)–(37).

4 Exponential-based method with two integrating factors

In this section, it is intended to concisely introduce the exponential-based integration with two factors, formerly presented in [30] followed by introducing a new semi-implicit integration. Moreover, the corresponding consistent tangent operators are derived. Using two integrating factors, the constitutive equations are transformed into two equivalent systems of differential equations as follows:

$$\begin{aligned} \dot{\mathbf{X}}_{\mathrm{a}} &= \mathbb{A}_{\mathrm{a}}\mathbf{X}_{\mathrm{a}}, \\ \dot{\mathbf{X}}_{\mathrm{b}} &= \mathbb{A}_{\mathrm{b}}\mathbf{X}_{\mathrm{b}}, \end{aligned} \tag{44}$$

$$\mathbf{X}_{\mathrm{a}} = \begin{Bmatrix} \mathbf{X}_{\mathrm{a}}^{\mathrm{s}} \\ X_{\mathrm{a}}^{0} \end{Bmatrix} = \begin{Bmatrix} X^0 \mathbf{s}' \\ X^0 R \end{Bmatrix}, \quad \mathbf{X}_{\mathrm{b}} = \begin{Bmatrix} X_{\mathrm{b}}^{1} \\ X_{\mathrm{b}}^{0} \end{Bmatrix} = \begin{Bmatrix} x^0(\tau_{\mathrm{y}} - \beta p') \\ x^0 R \end{Bmatrix}, \tag{45}$$

where the scalar parameters X^0 and x^0 are the integrating factors. Furthermore, the control matrixes $\mathbb{A}_{\mathrm{a}}$ and $\mathbb{A}_{\mathrm{a}}$ have the following forms:

$$\begin{aligned} \mathbb{A}_{\mathrm{a}} &= \frac{2G}{R} \begin{bmatrix} \mathbb{O}_{9\times 9}\ \dot{\mathbf{e}} \\ \dot{\mathbf{e}}^{\mathrm{T}} \quad 0 \end{bmatrix}_{10\times 10}, \\ \mathbb{A}_{\mathrm{b}} &= \frac{1}{R} \left[\left(\frac{1}{\sqrt{2}} \bar{Q} - 1 \right) \beta K \dot{\varepsilon}_{\mathrm{v}} + \bar{Q} G \mathbf{n}^{\mathrm{T}} \dot{\mathbf{e}} \right] \begin{bmatrix} 0 & 1 \\ 2 & 0 \end{bmatrix}, \end{aligned} \tag{46}$$

$$\bar{Q} = \frac{\sqrt{2} H_{\mathrm{iso}}}{\sqrt{2}(\bar{G} + \bar{K}\beta^2) R + H_{\mathrm{iso}}}. \tag{47}$$

In the last matrix, the vector $\mathbf{n}$ is normal to the yield surface, which is defined by $\mathbf{n} = \mathbf{s}'/R$. Furthermore, the factor x^0 has the form:

$$\boldsymbol{x}^0 = \exp(-2\bar{K}\beta^2 \gamma). \tag{48}$$

Moreover, X^0 and x^0 are connected to each other by:

$$x^0 = (X^0)^{-\frac{\bar{K}\beta^2}{\bar{G}}}. \tag{49}$$

4.1 Explicit integration algorithm with two factors (explicit-II)

Integrating the constitutive equations is started the same as the method presented in previous section. In fact, after computing the tentative solution, Eq. (18), the condition (19) needs to be verified checking whether or not the trial elastic solution is acceptable. If the condition is violated, the solution is not admissible and material undergoes the plastic behavior. As a result, one must determine the elastic and elastoplastic parts by means of the scalar parameter α. Having computed the stress contact point via Eq. (20) and adopting an explicit manner, the systems of differential equations (44) can be solved as:

$$\begin{aligned} \mathbf{X}_{\mathrm{a},n+1} &= \exp\left[\mathbb{A}_{\mathrm{a},n+\alpha}(1-\alpha)\Delta t\right] \mathbf{X}_{\mathrm{a},n+\alpha} = \mathbb{G}_{\mathrm{a},n+\alpha} \mathbf{X}_{\mathrm{a},n+\alpha}, \\ \mathbf{X}_{\mathrm{b},n+1} &= \exp\left[\mathbb{A}_{\mathrm{b},n+\alpha}(1-\alpha)\Delta t\right] \mathbf{X}_{\mathrm{b},n+\alpha} = \mathbb{G}_{\mathrm{b},n+\alpha} \mathbf{X}_{\mathrm{b},n+\alpha}, \end{aligned} \tag{50}$$

where the matrixes $\mathbb{G}_{\mathrm{a},n+\alpha}$ and $\mathbb{G}_{\mathrm{b},n+\alpha}$ have the following forms:

$$\begin{aligned} \mathbb{G}_{\mathrm{a},n+\alpha} &= \begin{bmatrix} \mathbb{I}_{9\times 9} + (a_{n+\alpha} - 1)\Delta\hat{\mathbf{e}}\Delta\hat{\mathbf{e}}^{\mathrm{T}} & b_{n+\alpha}\Delta\hat{\mathbf{e}}, \\ b_{n+\alpha}\Delta\hat{\mathbf{e}}^{\mathrm{T}} & a_{n+\alpha} \end{bmatrix}_{10\times 10}, \\ \mathbb{G}_{\mathrm{b}}, n+\alpha &= \begin{bmatrix} u_{n+\alpha} & \frac{1}{\sqrt{2}} v_{n+\alpha} \\ \sqrt{2} v_{n+\alpha} & u_{n+\alpha} \end{bmatrix}. \end{aligned} \tag{51}$$

While the scalars $a_{n+\alpha}$ and $b_{n+\alpha}$ have been provided by Eq. (23), $u_{n+\alpha}$ and $v_{n+\alpha}$ are described by the relations

$$\begin{aligned} u_{n+\alpha} &= \cosh(g_{n+\alpha}), \quad v_{n+\alpha} = \sinh(g_{n+\alpha}), \\ g_{n+\alpha} &= \frac{1}{R_{n+\alpha}} \left[\left(\frac{1}{\sqrt{2}} \bar{Q}_{n+\alpha} - 1 \right) \beta K \Delta\varepsilon_{\mathrm{v}} + G \bar{Q}_{n+\alpha} \mathbf{n}_{n+\alpha}^{\mathrm{T}} \Delta\mathbf{e} \right]. \end{aligned} \tag{52}$$

Subsequently, the integrating factor X^0 must be obtained. To reach this goal, Eq. (49) and the definitions of X_{a}^0 and X_{b}^0 are employed, yielding:

$$X_{n+1}^0 = \left(\frac{X_{\mathrm{a},n+1}^0}{X_{\mathrm{b},n+1}^0} \right)^{\frac{\bar{G}}{\bar{K}\beta^2 + \bar{G}}}. \tag{53}$$

Having X^0 at time t_{n+1}, it is possible to determine the deviatoric shifted stress and the radius of the yield surface through the following relations:

$$\mathbf{s}'_{n+1} = \frac{\mathbf{X}^{\mathrm{s}}_{\mathrm{a},n+1}}{X^0_{n+1}}, \tag{54}$$

$$R_{n+1} = \frac{X^0_{\mathrm{a},n+1}}{X^0_{n+1}}. \tag{55}$$

Finally, Eqs. (27) and (28) are exploited to update the yield stress and the center of the yield surface. Moreover, the hydrostatic pressure can be computed using Eq. (29).

4.2 Consistent tangent operator for explicit-II scheme

As mentioned before, the algorithmic (consistent) elastoplastic tangent operator is found by linearizing the stress updating algorithm. To meet this purpose, one needs to compute the expression $(\partial\boldsymbol{\sigma}/\partial\boldsymbol{\varepsilon})_{n+1}$ which results in calculating the derivative terms appearing in Eq. (31). In the aforementioned relation, the equation of the derivative $(\partial\mathbf{s}'/\partial\mathbf{e})_{n+1}$ would be practically the same as given by Eq. (32) replacing $\mathbf{X}^{\mathrm{s}}_{\mathrm{a},n+1}$ with $\mathbf{X}^{\mathrm{s}}_{n+1}$, as:

$$\frac{\partial\mathbf{s}'_{n+1}}{\partial\mathbf{e}_{n+1}} = \frac{1}{X^0_{n+1}}\frac{\partial\mathbf{X}^{\mathrm{s}}_{\mathrm{a},n+1}}{\partial\mathbf{e}_{n+1}} - \frac{\mathbf{X}^{\mathrm{s}}_{\mathrm{a},n+1}}{\left(X^0_{n+1}\right)^2}\left(\frac{\partial X^0_{n+1}}{\partial\mathbf{e}_{n+1}}\right)^{\mathrm{T}}. \tag{56}$$

The relation associated with X^0 in Eq. (53) is considered where taking its derivative with respect to $\mathbf{e}_{n+1}$ yields:

$$\frac{\partial X^0_{n+1}}{\partial\mathbf{e}_{n+1}} = \frac{\bar{G}}{\bar{K}\beta^2+\bar{G}}\frac{1}{X^0_{\mathrm{b},n+1}}\left(\frac{\partial X^0_{\mathrm{a},n+1}}{\partial\mathbf{e}_{n+1}} - \frac{X^0_{\mathrm{a},n+1}}{X^0_{\mathrm{b},n+1}}\frac{\partial X^0_{\mathrm{b},n+1}}{\partial\mathbf{e}_{n+1}}\right)\left(\frac{X^0_{\mathrm{a},n+1}}{X^0_{\mathrm{b},n+1}}\right)^{\frac{\bar{G}}{\bar{K}\beta^2+\bar{G}}-1}. \tag{57}$$

Having expanded Eqs. (50) and (51), one can reach $(\partial X^0_{\mathrm{a}}/\partial\mathbf{e})_{n+1}$ and $(\partial X^0_{\mathrm{b}}/\partial\mathbf{e})_{n+1}$ as follows:

$$\begin{aligned}\frac{\partial X^0_{\mathrm{a},n+1}}{\partial\mathbf{e}_{n+1}} &= \left(\Delta\hat{\mathbf{e}}^{\mathrm{T}}\mathbf{X}^{\mathrm{s}}_{\mathrm{a},n+\alpha}\right)\frac{\partial b_{n+\alpha}}{\partial\mathbf{e}_{n+1}} + b_{n+\alpha}\frac{\partial\Delta\hat{\mathbf{e}}}{\partial\mathbf{e}_{n+1}}\mathbf{X}^{\mathrm{s}}_{\mathrm{a},n+\alpha} + b_{n+\alpha}\frac{\partial\mathbf{X}^{\mathrm{s}}_{\mathrm{a},n+\alpha}}{\partial\mathbf{e}_{n+1}}\Delta\hat{\mathbf{e}}\\ &\quad + X^0_{\mathrm{a},n+\alpha}\frac{\partial a_{n+\alpha}}{\partial\mathbf{e}_{n+1}} + a_{n+\alpha}\frac{\partial X^0_{\mathrm{a},n+\alpha}}{\partial\mathbf{e}_{n+1}},\end{aligned} \tag{58}$$

$$\frac{\partial X^0_{\mathrm{b},n+1}}{\partial\mathbf{e}_{n+1}} = \sqrt{2}X^1_{\mathrm{b},n+\alpha}\frac{\partial v_{n+\alpha}}{\partial\mathbf{e}_{n+1}} + \sqrt{2}v_{n+\alpha}\frac{\partial X^1_{\mathrm{b},n+\alpha}}{\partial\mathbf{e}_{n+1}} + X^0_{\mathrm{b},n+\alpha}\frac{\partial u_{n+\alpha}}{\partial\mathbf{e}_{n+1}} + u_{n+\alpha}\frac{\partial X^0_{\mathrm{b},n+\alpha}}{\partial\mathbf{e}_{n+1}}. \tag{59}$$

For avoiding any confusion in tracking the main path, all derivatives in the above equations are provided in Appendix D. The only term left in Eq. (56) is $(\partial\mathbf{X}^{\mathrm{s}}_{\mathrm{a}}/\partial\mathbf{e})_{n+1}$. Taking the derivative of the relation related to $\mathbf{X}^{\mathrm{s}}_{\mathrm{a}}$ extracted from Eq. (50) brings about the following formula:

$$\begin{aligned}\frac{\partial\mathbf{X}^{\mathrm{s}}_{a,n+1}}{\partial\mathbf{e}_{n+1}} &= \frac{\partial\mathbf{X}^{\mathrm{s}}_{a,n+\alpha}}{\partial\mathbf{e}} + \left(\Delta\hat{\mathbf{e}}^{\mathrm{T}}\mathbf{X}^{\mathrm{s}}_{a,n+\alpha}\right)\Delta\hat{\mathbf{e}}\left(\frac{\partial a_{n+\alpha}}{\partial\mathbf{e}}\right)^{\mathrm{T}} + (a_{n+\alpha}-1)\left(\Delta\hat{\mathbf{e}}^{\mathrm{T}}\mathbf{X}^{\mathrm{s}}_{a,n+\alpha}\right)\frac{\partial\Delta\hat{\mathbf{e}}}{\partial\mathbf{e}}\\ &\quad + (a_{n+\alpha}-1)\Delta\hat{\mathbf{e}}\left(\frac{\partial\Delta\hat{\mathbf{e}}}{\partial\mathbf{e}}\mathbf{X}^{\mathrm{s}}_{a,n+\alpha}\right)^{\mathrm{T}} + (a_{n+\alpha}-1)\Delta\hat{\mathbf{e}}\left(\frac{\partial\mathbf{X}^{\mathrm{s}}_{a,n+\alpha}}{\partial\mathbf{e}}\Delta\hat{\mathbf{e}}\right)^{\mathrm{T}}\\ &\quad + (a_{n+\alpha}-1)\Delta\hat{\mathbf{e}}\left(\frac{\partial\mathbf{X}^{\mathrm{s}}_{a,n+\alpha}}{\partial\mathbf{e}}\Delta\hat{\mathbf{e}}\right)^{\mathrm{T}} + X^0_{a,n+\alpha}\Delta\hat{\mathbf{e}}\left(\frac{\partial b_{n+\alpha}}{\partial\mathbf{e}}\right) + b_{n+\alpha}X^0_{a,n+\alpha}\frac{\partial\Delta\hat{\mathbf{e}}}{\partial\mathbf{e}}\\ &\quad + b_{n+\alpha}\Delta\hat{\mathbf{e}}\left(\frac{\partial X^0_{a,n+\alpha}}{\partial\mathbf{e}}\right).\end{aligned} \tag{60}$$

The derivative terms in the former equation are presented in Appendix D. It should be noted that the terms $(\partial\boldsymbol{\alpha}/\partial\mathbf{e})_{n+1}$ and $(\partial p/\partial\boldsymbol{\varepsilon})_{n+1}$ were previously mentioned in Sect. 3.2.

4.3 Semi-implicit integration algorithm with two factors (semi-implicit-II)

It is desired to develop a semi-implicit scheme for exponential-based integration with two factors. To meet this purpose, the matrixes $\mathbb{G}_{\mathrm{a}}$ and $\mathbb{G}_{\mathrm{b}}$ must be computed at time $t = t_{n+r(1-\alpha)}$ within the elastoplastic interval of the time step rather than at the beginning point, which is normally performed in the fully explicit scheme. Essentially, the variables R and $\mathbf{n}$ have to be found at time $t = t_{n+r(1-\alpha)}$. In view of that, one could employ Eq. (50) at time $t = t_{n+r(1-\alpha)}$ as:

$$\begin{aligned}\mathbf{X}_{\mathrm{a},n+r(1-\alpha)} &= \exp\left[\mathbb{A}_{\mathrm{a},n+\alpha} r(1-\alpha)\Delta t\right]\mathbf{X}_{\mathrm{a},n+\alpha} = \bar{\mathbb{G}}_{\mathrm{a},n+\alpha}\mathbf{X}_{\mathrm{a},n+\alpha},\\ \mathbf{X}_{\mathrm{b},n+r(1-\alpha)} &= \exp\left[\mathbb{A}_{\mathrm{b},n+\alpha} r(1-\alpha)\Delta t\right]\mathbf{X}_{\mathrm{b},n+\alpha} = \bar{\mathbb{G}}_{\mathrm{b},n+\alpha}\mathbf{X}_{\mathrm{b},n+\alpha}.\end{aligned} \tag{61}$$

By utilizing the results of the last solutions, one obtains the following relations:

$$\begin{aligned}\mathbf{n}_{n+r(1-\alpha)} &= \frac{\mathbf{X}^{\mathrm{s}}_{a,n+r(1-\alpha)}}{X^0_{a,n+r(1-\alpha)}},\\ R_{n+r(1-\alpha)} &= \frac{X^0_{a,n+r(1-\alpha)}}{X^0_{n+r(1-\alpha)}},\\ X^0_{n+r(1-\alpha)} &= \left(\frac{X^0_{a,n+r(1-\alpha)}}{X^0_{b,n+r(1-\alpha)}}\right)^{\frac{\bar{G}}{\bar{K}\beta^2+\bar{G}}}.\end{aligned} \tag{62}$$

In these equations, $\mathbf{X}^{\mathrm{s}}_{a,n+r(1-\alpha)}$, $X^0_{a,n+r(1-\alpha)}$ and $X^0_{b,n+r(1-\alpha)}$ are given by:

$$\begin{aligned}\mathbf{X}^{\mathrm{s}}_{a,n+r(1-\alpha)} &= \mathbf{X}^{\mathrm{s}}_{a,n+\alpha} + \left[(\bar{a}_{n+\alpha}-1)\Delta\hat{\mathbf{e}}^{\mathrm{T}}\mathbf{X}^{\mathrm{s}}_{a,n+\alpha}\right]\Delta\hat{\mathbf{e}} + \bar{b}_{n+\alpha}X^0_{n+\alpha}\Delta\hat{\mathbf{e}},\\ X^0_{a,n+r(1-\alpha)} &= \bar{b}_{n+\alpha}\Delta\hat{\mathbf{e}}^{\mathrm{T}}\mathbf{X}^{\mathrm{s}}_{a,n+\alpha} + \bar{a}_{n+\alpha}X^0_{n+\alpha},\\ X^0_{b,n+r(1-\alpha)} &= \sqrt{2}\bar{v}_{n+\alpha}X^1_{b,n+\alpha} + \bar{u}_{n+\alpha}X^0_{b,n+\alpha}.\end{aligned} \tag{63}$$

In addition, the scalar parameters $\bar{u}_{n+\alpha}$ and $\bar{v}_{n+\alpha}$ are defined as

$$\begin{aligned}\bar{u}_{n+\alpha} &= \cosh(rg_{n+\alpha}),\\ \bar{v}_{n+\alpha} &= \sinh(rg_{n+\alpha}).\end{aligned} \tag{64}$$

Once the parameters $R_{n+r(1-\alpha)}$ and $\mathbf{n}_{n+r(1-\alpha)}$ are clear, the matrixes $\mathbb{G}_{\mathrm{a}}$ and $\mathbb{G}_{\mathrm{b}}$ can be calculated as follows:

$$\begin{aligned}\mathbf{X}_{a,n+1} &= \exp\left[\mathbb{A}_{a,n+r(1-\alpha)}(1-\alpha)\Delta t\right]\mathbf{X}_{a,n+\alpha} = \mathbb{G}_{a,n+r(1-\alpha)}\mathbf{X}_{a,n+\alpha},\\ \mathbf{X}_{b,n+1} &= \exp\left[\mathbb{A}_{b,n+r(1-\alpha)}(1-\alpha)\Delta t\right]\mathbf{X}_{b,n+\alpha} = \mathbb{G}_{b,n+r(1-\alpha)}\mathbf{X}_{b,n+\alpha},\end{aligned} \tag{65}$$

$$\begin{aligned}\mathbb{G}_{a,n+r(1-\alpha)} &= \begin{bmatrix}\mathbb{I}_{9\times9} + (a_{n+r(1-\alpha)}-1)\Delta\hat{\mathbf{e}}\Delta\hat{\mathbf{e}}^{\mathrm{T}} & b_{n+r(1-\alpha)}\Delta\hat{\mathbf{e}}\\ b_{n+r(1-\alpha)}\Delta\hat{\mathbf{e}}^{\mathrm{T}} & a_{n+r(1-\alpha)}\end{bmatrix}_{10\times10},\\ \mathbb{G}_{b,n+r(1-\alpha)} &= \begin{bmatrix}u_{n+r(1-\alpha)} & \frac{1}{\sqrt{2}}v_{n+r(1-\alpha)}\\ \sqrt{2}v_{n+r(1-\alpha)} & u_{n+r(1-\alpha)}\end{bmatrix}.\end{aligned} \tag{66}$$

The scalars $a_{n+r(1-\alpha)}$ and $b_{n+r(1-\alpha)}$ were introduced in Eq. (43). Also, the scalars $u_{n+r(1-\alpha)}$ and $v_{n+r(1-\alpha)}$ are given through the following relations:

$$\begin{aligned}u_{n+r(1-\alpha)} &= \cosh\left(g_{n+r(1-\alpha)}\right),\\ v_{n+r(1-\alpha)} &= \sinh\left(g_{n+r(1-\alpha)}\right),\\ g_{n+r(1-\alpha)} &= \frac{1}{R_{n+r(1-\alpha)}}\left[\left(\frac{1}{\sqrt{2}}\bar{Q}_{n+r(1-\alpha)}-1\right)\beta K\Delta\varepsilon_{\mathrm{v}} + G\bar{Q}_{n+r(1-\alpha)}\mathbf{n}^{\mathrm{T}}_{n+r(1-\alpha)}\Delta\mathbf{e}\right].\end{aligned} \tag{67}$$

Note that the rest of the stress updating process is the same as given in Sect. 4.1.

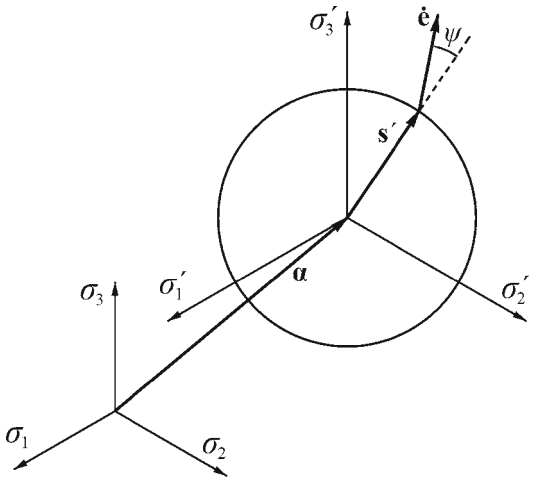

Fig. 2 Definition of angle ψ

4.4 Consistent tangent operator for semi-implicit-II scheme

In order to derive the consistent tangent operator, the stress updating algorithm has to be linearized. Therefore, the derivative $(\partial\boldsymbol{\sigma}/\partial\boldsymbol{\varepsilon})_{n+1}$ as given in Eq. (30) or (31) must be computed, which means calculating the terms $(\partial\mathbf{s}'/\partial\mathbf{e})_{n+1}$, $(\partial\boldsymbol{\alpha}/\partial\mathbf{e})_{n+1}$ and $(\partial p/\partial\boldsymbol{\varepsilon})_{n+1}$. The main relation for $(\partial\mathbf{s}'/\partial\mathbf{e})_{n+1}$ and the associated derivatives were presented in Eqs. (58)–(60). However, these relations need a little modification, which is replacing the subscript $n+\alpha$ with $n+r(1-\alpha)$ for the scalars a, b, u and v. Furthermore, the derivatives of the aforementioned scalars are provided in Appendix E. In addition, the derivatives of the back stress and hydrostatic pressure with respect to strain were given in the previous sections.

5 Accurate integration

An accurate integration method was presented for the prescribed constitutive equations in Reference [30]. Considering the elastoplastic phase, this method uses the definition of the angle between the stress state and the strain rate in the deviatoric plane as:

$$\mathbf{s}'^{\mathrm{T}}\dot{\mathbf{e}} = R||\dot{\mathbf{e}}||\cos\psi. \tag{68}$$

The angle ψ is shown in Fig. 2. Taking into account the constant strain rate assumption and using Eq. (68), the original constitutive equations can be transformed into the following ordinary differential equations (ODEs):

$$\dot{\mathbf{Y}} = \mathbf{F}(t, \mathbf{Y}), \tag{69}$$

$$\begin{aligned}
\mathbf{Y} &:= \left\{ \begin{array}{c} y_1 \\ y_2 \end{array} \right\} = \left\{ \begin{array}{c} R \\ \psi \end{array} \right\}, \\
\mathbf{F} &:= \left\{ \begin{array}{c} f_1 \\ f_2 \end{array} \right\} = \left\{ \begin{array}{c} 2G||\dot{\mathbf{e}}||\cos y_2 - \frac{2\bar{G}y_1}{H_{\mathrm{iso}}+\sqrt{2}(\bar{G}+\bar{K}\beta^2)y_1}(\sqrt{2}G||\dot{\mathbf{e}}||\cos y_2 + \beta K\dot{\varepsilon}_{\mathrm{v}}) \\ -\frac{2G||\dot{\mathbf{e}}||\sin y_2}{y_1} \end{array} \right\}.
\end{aligned} \tag{70}$$

Basically, the heart of the accurate integration is solving the last ODEs. Having no closed-form solution for the aforementioned differential equations, it is necessary to utilize an accurate numerical technique namely the fifth-order Runge–Kutta method. Since in this part, the main goal is to derive the algorithmic consistent tangent operator for the accurate integration, it would be suitable to concisely review and have the integration algorithm presented in the next section.

5.1 Integration algorithm

Since the accurate integration is, in effect, an explicit method, it can be started in each load step with an elastic trial solution, Eq. (18), and followed by checking the condition (19). Subsequently, if the load step has entered the elastoplastic phase, the parameter α is used to find the contact point by means of Eq. (20). Once the stress has reached the elastic boundary, one needs to compute the following initial values to solve Eq. (69):

$$\begin{aligned} R_{n+\alpha} &= \sqrt{2}(\tau_{y,n} - \beta p'_{n+\alpha}), \\ \psi_{n+\alpha} &= \cos^{-1}\left(\frac{\mathbf{s}'^{\mathrm{T}}_{n+\alpha}\Delta\mathbf{e}}{R_{n+\alpha}\,\|\Delta\mathbf{e}\|}\right). \end{aligned} \tag{71}$$

At this stage, using the fifth-order Dormand-Prince technique [43] contributes to finding the scalars R and ψ at the end of the load step, at time t_{n+1}. Afterward, the deviatoric shifted stress at time t_{n+1} can be determined by linearly combining the deviatoric shifted stress at time $t_{n+\alpha}$ and the increment of the trial stress as

$$\mathbf{s}'_{n+1} = \xi\mathbf{s}'_{n+\alpha} + \zeta\Delta\mathbf{s}'^{\mathrm{TR}}, \tag{72}$$

where $\Delta\mathbf{s}'^{\mathrm{TR}} = 2G(1-\alpha)\Delta\mathbf{e}$, and the scalars ξ and ζ are given by

$$\begin{aligned} \xi &= \frac{R_{n+1}\sin\psi_{n+1}}{R_{n+\alpha}\sin\psi_{n+\alpha}}, \\ \zeta &= \frac{R_{n+1}\sin(\psi_{n+\alpha} - \psi_{n+1})}{||\Delta\mathbf{s}'^{\mathrm{TR}}||\sin\psi_{n+\alpha}}. \end{aligned} \tag{73}$$

It should be mentioned the other variables may be updated as in the previous sections.

5.2 Consistent tangent operator for accurate integration

Bearing Eqs. (31), (72) and (73) in mind, it is obvious that the derivatives R_{n+1} and ψ_{n+1} with respect to $\mathbf{e}_{n+1}$, i.e. $(\partial\mathbf{Y}/\partial\mathbf{e})_{n+1}$, must be computed. Therefore, to obtain the aforementioned derivative vector, it is necessary to derive its governing differential equations as:

$$\frac{\mathrm{d}}{\mathrm{d}t}\left(\frac{\partial\mathbf{Y}}{\partial\mathbf{e}}\right) = \frac{\partial\mathbf{F}}{\partial\mathbf{Y}}\frac{\partial\mathbf{Y}}{\partial\mathbf{e}}. \tag{74}$$

Therefore, it is convenient to define the vectors

$$\mathbf{G} := \left\{\begin{matrix} g_1 \\ g_2 \end{matrix}\right\} = \left\{\begin{matrix} \partial y_1/\partial\mathbf{e} \\ \partial y_2/\partial\mathbf{e} \end{matrix}\right\} = \frac{\partial\mathbf{Y}}{\partial\mathbf{e}} \tag{75}$$

and

$$\mathbf{Q} := \left\{\begin{matrix} \mathbf{q}_1 \\ \mathbf{q}_2 \end{matrix}\right\} = \left\{\begin{matrix} (\partial f_1/\partial y_1)\,(\partial y_1/\partial\mathbf{e}) + (\partial f_1/\partial y_2)\,(\partial y_2/\partial\mathbf{e}) \\ (\partial f_2/\partial y_1)\,(\partial y_1/\partial\mathbf{e}) + (\partial f_2/\partial y_2)\,(\partial y_2/\partial\mathbf{e}) \end{matrix}\right\} = \frac{\partial\mathbf{F}}{\partial\mathbf{Y}}\frac{\partial\mathbf{Y}}{\partial\mathbf{e}}. \tag{76}$$

Now, the differential equations (74) may be rewritten as

$$\dot{\mathbf{G}} = \mathbf{Q}. \tag{77}$$

Consequently, the constitutive variables and their derivatives can simultaneously be found solving the former ODEs along with the system of ODEs given in Eq. (69). In fact, for preserving the quadratic rate of the asymptotic convergence of the Newton iterations in the global solution of the finite element analysis, it is necessary that the following system of ODEs be solved in each load step and the corrective iterations at each Gauss point:

$$\left\{\begin{matrix} \dot{\mathbf{Y}} \\ \dot{\mathbf{G}} \end{matrix}\right\} = \left\{\begin{matrix} \mathbf{F} \\ \mathbf{Q} \end{matrix}\right\}. \tag{78}$$

The derivatives $(\partial\boldsymbol{\alpha}/\partial\mathbf{e})_{n+1}$ and $(\partial p/\partial\boldsymbol{\varepsilon})_{n+1}$ have been addressed in the previous sections. For calculating $(\partial\mathbf{s}'/\partial\mathbf{e})_{n+1}$, Eq. (72) must be used:

$$\frac{\partial\mathbf{s}'_{n+1}}{\partial\mathbf{e}_{n+1}}=\mathbf{s}'_{n+\alpha}\left(\frac{\partial\xi}{\partial\mathbf{e}_{n+1}}\right)^{\mathrm{T}}+\xi\frac{\partial\mathbf{s}'_{n+\alpha}}{\partial\mathbf{e}_{n+1}}+\Delta\mathbf{s}'^{\mathrm{TR}}\left(\frac{\partial\zeta}{\partial\mathbf{e}_{n+1}}\right)^{\mathrm{T}}+\zeta\frac{\partial\Delta\mathbf{s}'^{\mathrm{TR}}}{\partial\mathbf{e}_{n+1}}. \tag{79}$$

The derivatives left unknown in this section are given in Appendix F.

6 Numerical tests

In the previous sections, two improved exponential-based integrations were presented. In addition, the consistent tangent operators were obtained for the aforementioned schemes and also two fully explicit exponential tactics. Finally, the derivation approach and the formulations for the consistent tangent operator of the accurate integration were discussed. Hence, numerical tests should be comprised of the assessments of the accuracy and precision order for the new techniques, and the examination of the derived consistent tangent operators. The former appraisal could be achieved by updating the stress and the internal variables for known strain paths in the Gauss point scale. Moreover, using the iso-error maps, which are strong tools for evaluating the accuracy in detail, could be appropriate. On the other hand, solving the boundary value problems may be needed for testing the consistent tangent operators. In fact, achieving the quadratic convergence rate in the implicit finite element codes, which commonly use the Newton-Raphson approach, is the proof of the correctness of the consistent tangent operator. In what follows, all mentioned tests are provided to acquire a comprehensive evaluation.

For convenience, the following abbreviations are used for the numerical integrations in question throughout the numerical studies:

I- **FEX-I**: Fully EXplicit exponential-based integration with ONE integrating factor.
II- **FEX-II**: Fully EXplicit exponential-based integration with TWO integrating factors.
III- **SIM-I**: Semi-IMplicit exponential-based integration with ONE integrating factor.
IV- **SIM-II**: Semi-IMplicit exponential-based integration with TWO integrating factors.
V- **AC**: ACcurate integration.

Furthermore, in all numerical tests, the integration parameter 'r' of SIM-I and SIM-II schemes, which characterizes the specific time in the middle of the elastoplastic part of the load step, is chosen equal to 1/2. It is clear that choosing other values for the aforementioned parameter yields other results with different accuracies, but it is obvious that $r=1/2$ is a rational choice for all conditions.

6.1 Strain load histories

Two strain-controlled histories are considered, which are non-proportional. In these histories, two components ε_{11} and ε_{12} are varied proportionally to $\varepsilon_{y0}=\sqrt{3}(\tau_{y0}/E)$ as shown in Figs. 3 and 4, whereas the other components of the strain are kept equal to zero. It should be mentioned that in order to eliminate the error of the discretization of the load path, the strain load histories have been considered in a linear manner. Moreover, the mechanical properties of the material are taken into account as:

$$E=1.125\ \text{s.u. (stress unit)},\quad \nu=0.125,\quad \tau_{\mathrm{y0}}=0.633\ \text{s.u.},\quad \beta=0.366,$$
$$H_{\mathrm{kin}}=1\ \text{s.u.},\quad H_{\mathrm{iso}}=0.134\ \text{s.u.}^2$$

The stresses updated by the accurate integration presented in Sect. 5 are chosen as exact results, $\boldsymbol{\sigma}_n^{\mathrm{E}}$, and are utilized to compute the error of the other integrations under discussion. The fifth-order Dormand-Prince method together with $\Delta t=0.01$ sec is adopted to solve the system of ODEs (69). On the other hand, the stresses, $\boldsymbol{\sigma}_n^{\mathrm{N}}$, are updated via the exponential-based integration schemes for the practical step size of $\Delta t=0.1$ sec. Finally, the stress relative errors are computed by means of the following relation:

$$E_n^{\boldsymbol{\sigma}}=\frac{\left\|\boldsymbol{\sigma}_n^{\mathrm{E}}-\boldsymbol{\sigma}_n^{\mathrm{N}}\right\|}{\left\|\boldsymbol{\sigma}_n^{\mathrm{E}}\right\|}. \tag{80}$$

The stress relative errors of the schemes are plotted for two strain load histories 1 and 2, respectively, in Figs. 5 and 6. According to these figures, the errors of the new semi-implicit schemes are very low in comparison

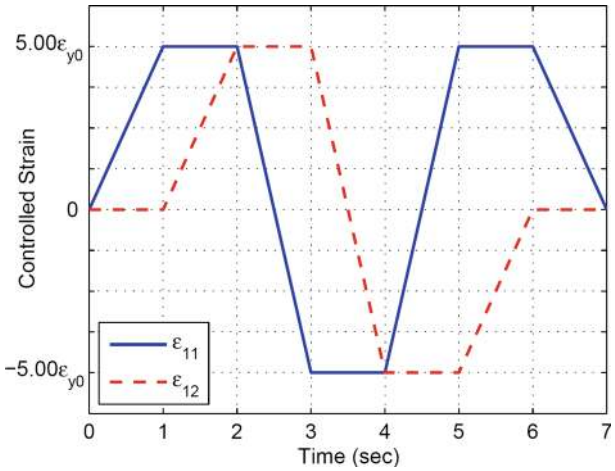

Fig. 3 Strain load history 1

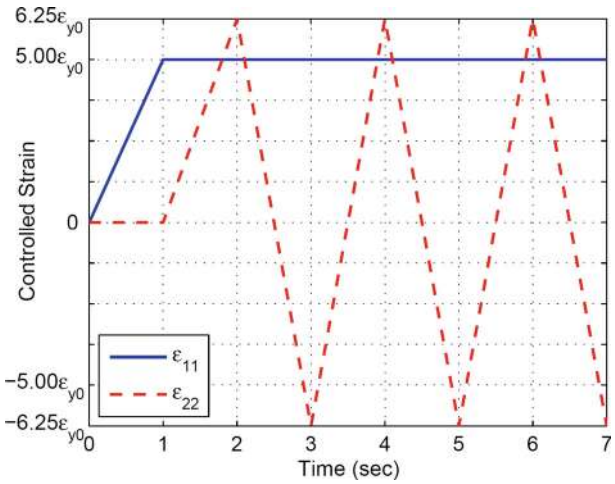

Fig. 4 Strain load history 2

to the fully explicit ones. In other words, the results indicate that the accuracy of the explicit schemes has noticeably been improved by implementing the semi-implicit technique. In fact, evaluating the variables of the control matrixes, Eqs. (14) and (44), at the specific time in the middle of the elastoplastic part of the time step leads to far more accurate answers. Besides, the SIM-II scheme turns out to be the most accurate integration in both diagrams of the results.

In the rest of the section, the convergence rates of the schemes are examined by computing the errors for different time-step sizes. To reach this goal, the average error is computed using the following relationship:

$$E_{\mathrm{A}}^{\sigma} = \frac{1}{N} \sum_{n=1}^{N} \frac{\left\| \boldsymbol{\sigma}_n^{\mathrm{E}} - \boldsymbol{\sigma}_n^{\mathrm{N}} \right\|}{\left\| \boldsymbol{\sigma}_n^{\mathrm{E}} \right\|}. \tag{81}$$

In the above equation, the total number of the time steps is denoted by N. Figures 7 and 8 display, respectively, the average errors for strain load histories 1 and 2 for different time steps by the schemes under consideration. For convenience, the logarithmic space is used to show the results. Evidently, the slope of each line indicates the convergence rate of the integrations. From these diagrams, it can be observed that both semi-implicit schemes have second-order accuracy, while the accuracy rates of both fully explicit techniques are linear. It should be noted that having second-order accuracy is not a basic requirement for a stress updating scheme, nevertheless it is a desirable characteristic.

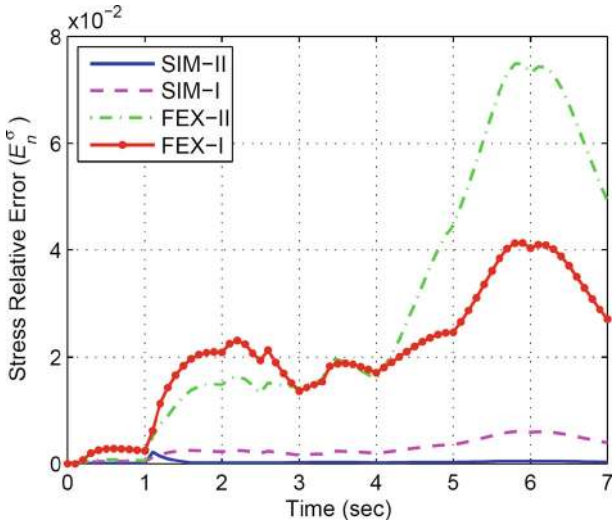

Fig. 5 Stress relative error of different schemes for strain load history 1 with $\Delta t = 0.1\,\mathrm{s}$

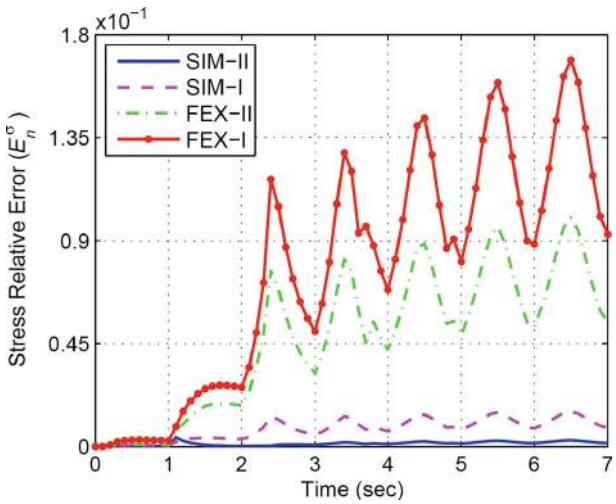

Fig. 6 Stress relative error of different schemes for strain load history 2 with $\Delta t = 0.1\,\mathrm{s}$

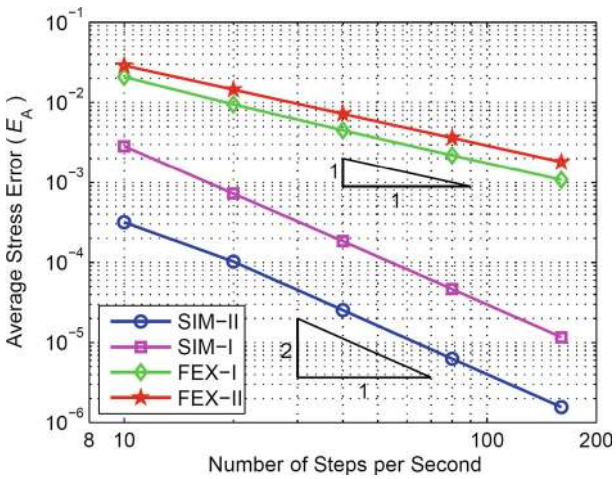

Fig. 7 Average stress error of different schemes for strain load history 1

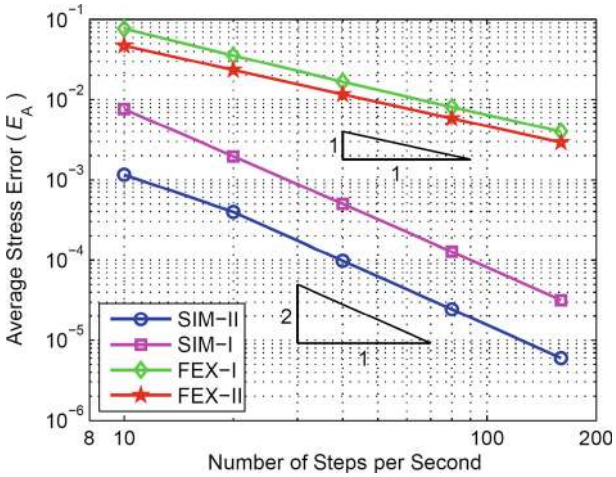

Fig. 8 Average stress error of different schemes for strain load history 2

6.2 Iso-error maps

In the previous subsection, the accuracies of the schemes were generally studied. Here, it is intended to assess the accuracy in depth by testing the radial accuracy and angular accuracy separately. For that reason, the iso-error maps are utilized as powerful means. To compute the error contours, as a standard methodology, it is firstly considered that the stress point is located on the yield surface at the generic time $t = t_n$. It follows that a strain increment in the deviatoric plane, $\Delta\mathbf{e}$, is arbitrarily selected while it has the principal directions the same as the shifted stress at time $t = t_n$, i.e. $\mathbf{s}'_n$. On the other hand, for having a specific strain vector, i.e. $\Delta\boldsymbol{\varepsilon}$, the volumetric part of the strain, $\Delta\varepsilon_v$, should be characterized as well as the deviatoric part. To do that, one could choose a value for the parameter V, which is in effect a relation between the magnitude of the increments of the deviatoric strain and the volumetric strain part. By a numerical method and also an exact solution, the final stress, at time $t = t_{n+1}$, should be determined to compute the errors of the numerical techniques. These computations are carried out for a wide range of strain increments. In fact, a range of the deviatoric strain vectors having the principle deviatoric plane, likewise, the deviatoric plane of $\mathbf{s}'_n$ are selected and determined through the normal and tangent projections as:

$$\begin{aligned} N &= \rho \cos\psi_n, \\ T &= \rho \sin\psi_n, \end{aligned} \tag{82}$$

where the scale parameter ρ is defined by

$$\rho = \frac{G\,\|\Delta\mathbf{e}\|}{5R_n}. \tag{83}$$

At this stage, it is appropriate to illustrate the definitions of N and T in Fig. 9 for the sake of clarity. Therefore, a strain vector, $\Delta\boldsymbol{\varepsilon}$, could be uniquely characterized by selecting the values of the parameters N, T and V. In order to present the results of the analyses, the radial and angular errors are defined and computed via the following relationships:

$$\begin{aligned} \Delta\theta &= \cos^{-1}\left(\frac{\left(\mathbf{s}'^{\mathrm{E}}_{n+1}\right)^{\mathrm{T}}\mathbf{s}'^{\mathrm{N}}_{n+1}}{R^{\mathrm{E}}_{n+1}R^{\mathrm{N}}_{n+1}}\right), \\ \Delta R &= \left(\frac{R^{\mathrm{E}}_{n+1} - R^{\mathrm{N}}_{n+1}}{R^{\mathrm{E}}_{n+1}}\right) \times 100\,\%. \end{aligned} \tag{84}$$

In these equalities, $\Delta\theta$ and ΔR represent the angular error and the radial error, respectively. As was addressed before, the stresses and radiuses of the yield surface denoted by the superscripts 'E' and 'N' are computed

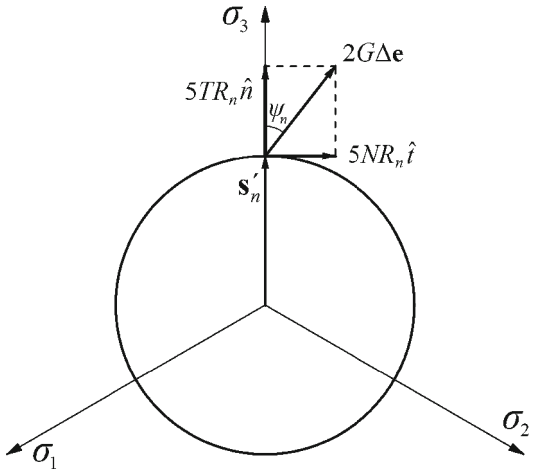

Fig. 9 Definition of the parameters N and T

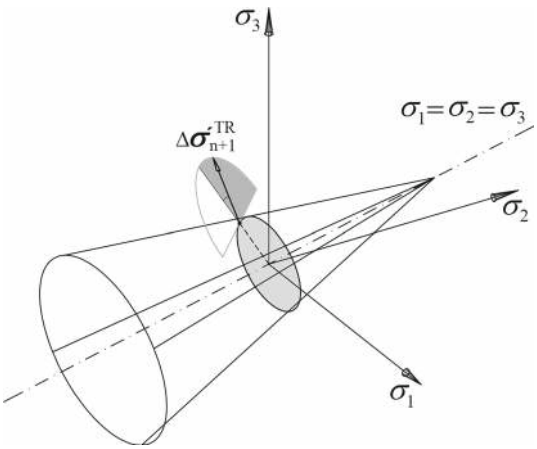

Fig. 10 The status of the trial stress in the principle stresses space for $V = 0$

through the accurate integration (AC) and the numerical integrations based on exponential maps, respectively. In order to plot the iso-error maps, two different values of $V = 0$ and $V = 1$ are adopted. Furthermore, the following domains for N and T are selected:

$$0 \le N \le 5, \quad 0 \le T \le 5 \quad \text{for } V = 0,$$
$$-5 \le N \le 5, \quad 0 \le T \le 5 \quad \text{for } V = 1.$$

It is worth mentioning that in the case of $V = 0$ the increment of the trial stress, i.e. $2G\Delta\mathbf{e}$, occurs in the deviatoric plane (Fig. 10). Therefore, staying in the plastic phase requires that N not have negative values, and as is shown in Fig. 11, the angle ψ_n change from 0 to $\pi/2$. For $V = 1$, the increment of the trial stress is located on the tangent plane to the yield surface as presented in Fig. 12. As a result, N could take the negative value as well as the positive ones and ψ_n could take the angles from 0 to π (Fig. 13). Moreover, the material properties are assumed the same as in the previous section.

Finally, the contours of the errors are plotted in Figs. 14–29. In all diagrams, the error areas with the absolute value of errors larger than 0.5 % and 0.5° have been shadowed for convenience. Considering the case of $V = 0$ and the angular errors in Figs. 14, 15, 16, 17, it is obvious that the SIM-I and SIM-II schemes present a very small angular error compared to the FEX-I and FEX-II schemes, as the maximum errors 0.82° and 0.90°of the FEX-I and FEX-II schemes have been reduced to 0.08° and 0.16° with the SIM-I and SIM-II schemes. Furthermore, the minimum angular error in this case is related to the SIM-I. For $V = 0$, the radial error contours presented in Figs. 18, 19, 20, 21 illustrate the distinct accuracy of the improved schemes, i.e. SIM-I and SIM-II. From these diagrams, it can be observed that the maximum errors for the aforementioned schemes are limited to 0.26 and 0.14 % for the SIM-I and SIM-II, respectively.

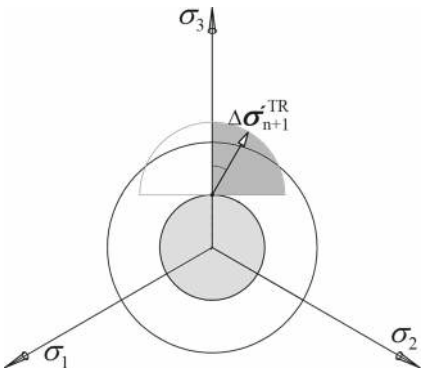

Fig. 11 The status of the trial stress in the deviatoric plane for $V = 0$

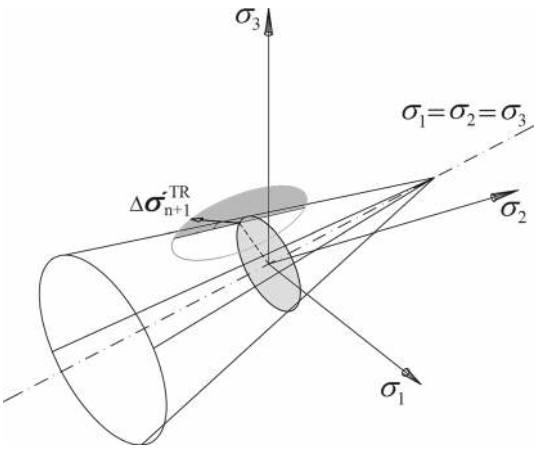

Fig. 12 The status of the trial stress in the principle stresses space for $V = 1$

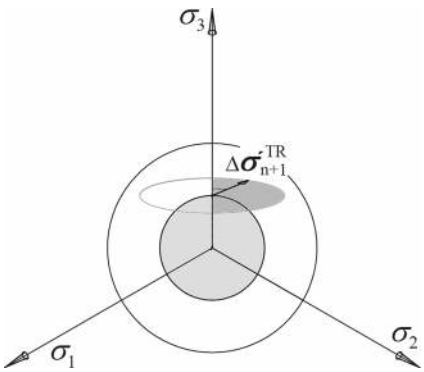

Fig. 13 The status of the trial stress in the deviatoric plane for $V = 1$

Figures 22, 23, 24, 25 are corresponding to $V = 1$ and the angular errors. The figures show that the maximum angular errors of SIM-I and SIM-II are about 5.5° and significantly smaller than the maximum errors of about 15.5° related to FEX-I and FEX-II. In addition, the hatched areas have been reduced for SIM-I and SIM-II compared to FEX-I and FEX-II. Finally, Figs. 26, 27, 28, 29 disclose the radial errors for the case of $V = 1$. As can be seen from the diagrams, the maximum errors along with the hatched areas for the improved schemes (SIM-I and SIM-II) have noticeably been moderated with respect to FEX-I and FEX-II. The enhancement for the hatched area of the SIM-II method is more evident. In fact, considering the same accuracy of the analysis, the domain of the increment loads for the SIM-II has been really extended with respect to the domain corresponding to FEX-II. In general, from all diagrams, it can be concluded that the scheme SIM-II has the best precision.

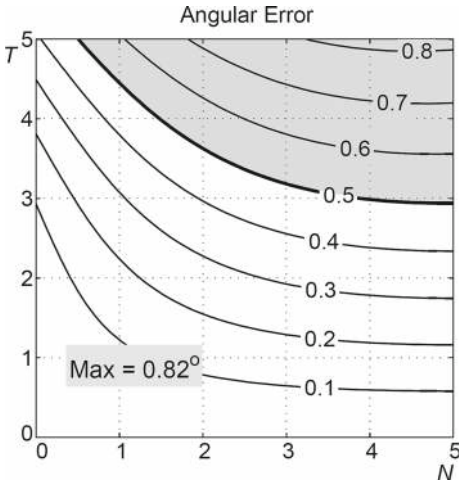

Fig. 14 The angular error for FEX-I, $V = 0$

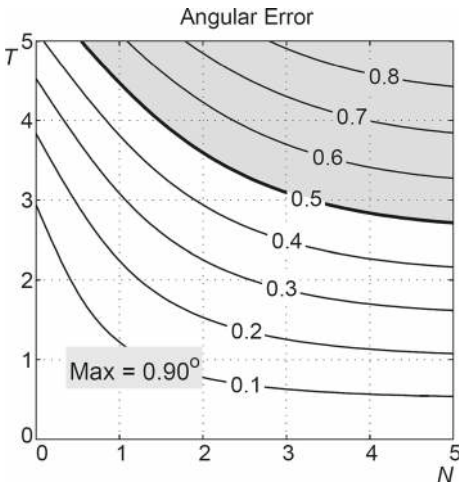

Fig. 15 The angular error for FEX-II, $V = 0$

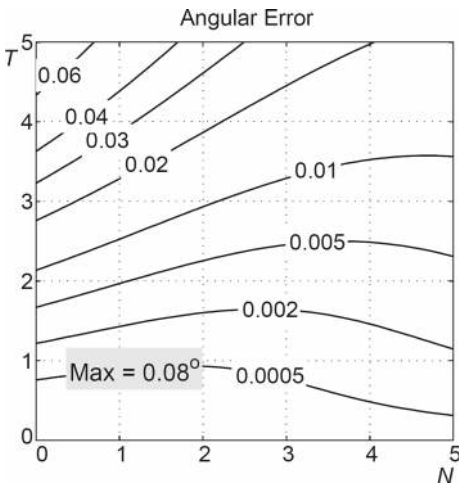

Fig. 16 The angular error for SIM-I, $V = 0$

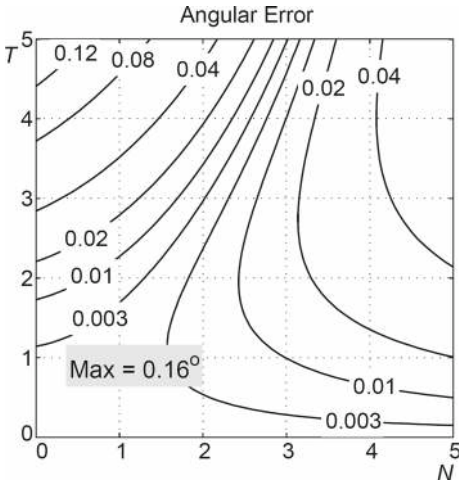

Fig. 17 The angular error for SIM-II, $V = 0$

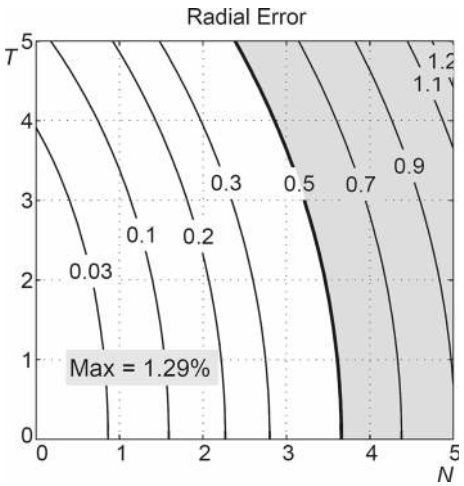

Fig. 18 The radial error for FEX-I, $V = 0$

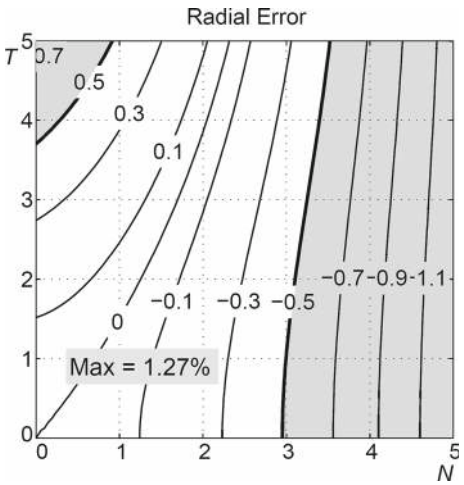

Fig. 19 The radial error for FEX-II, $V = 0$

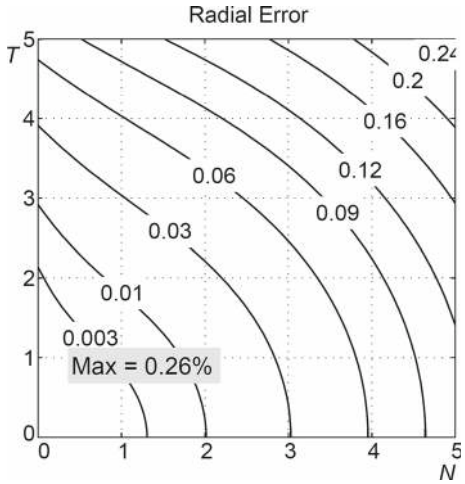

Fig. 20 The radial error for SIM-I, $V = 0$

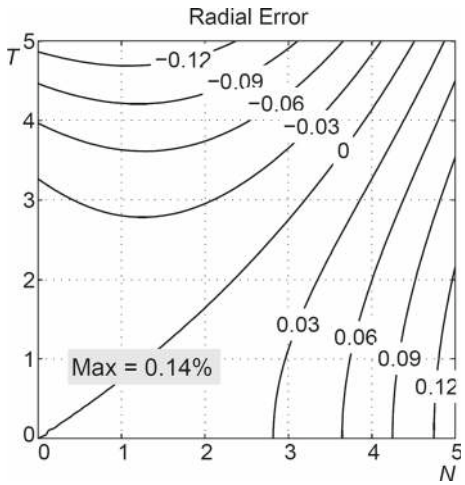

Fig. 21 The radial error for SIM-II, $V = 0$

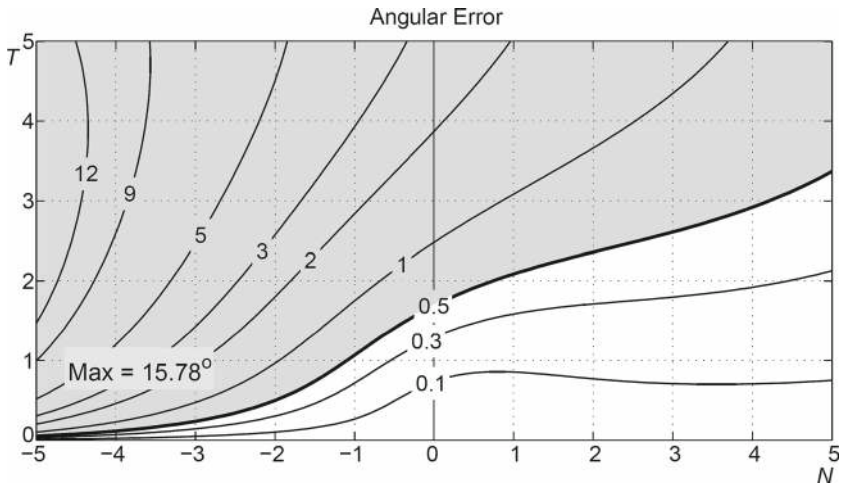

Fig. 22 The angular error for FEX-I, $V = 1$

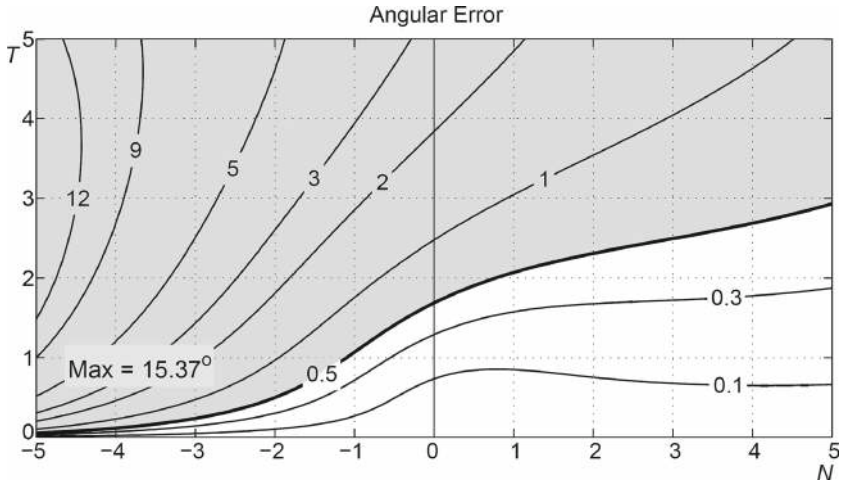

Fig. 23 The angular error for FEX-II, $V = 1$

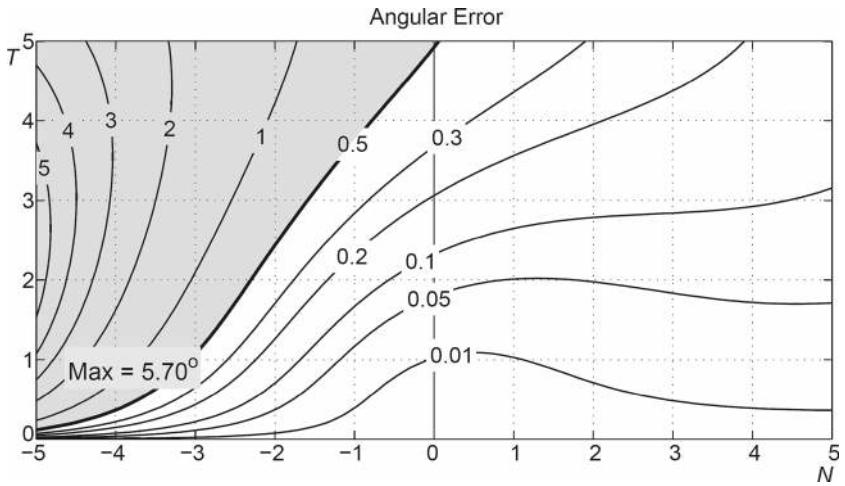

Fig. 24 The angular error for SIM-I, $V = 1$

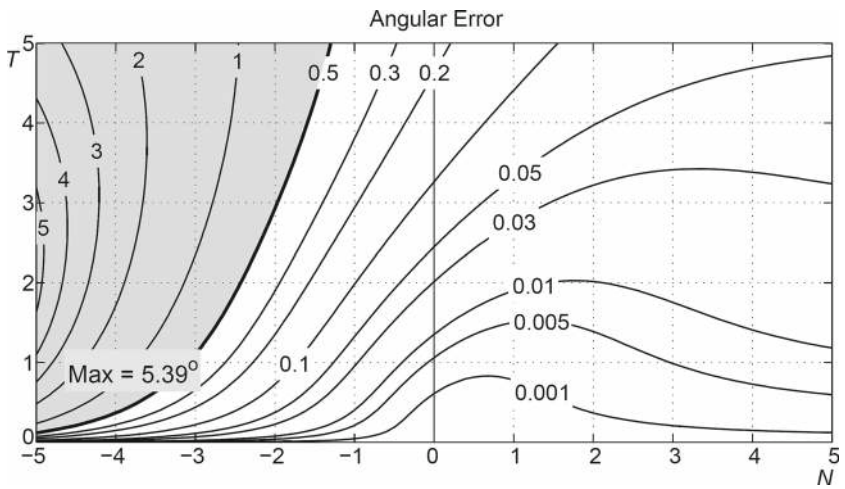

Fig. 25 The angular error for SIM-II, $V = 1$

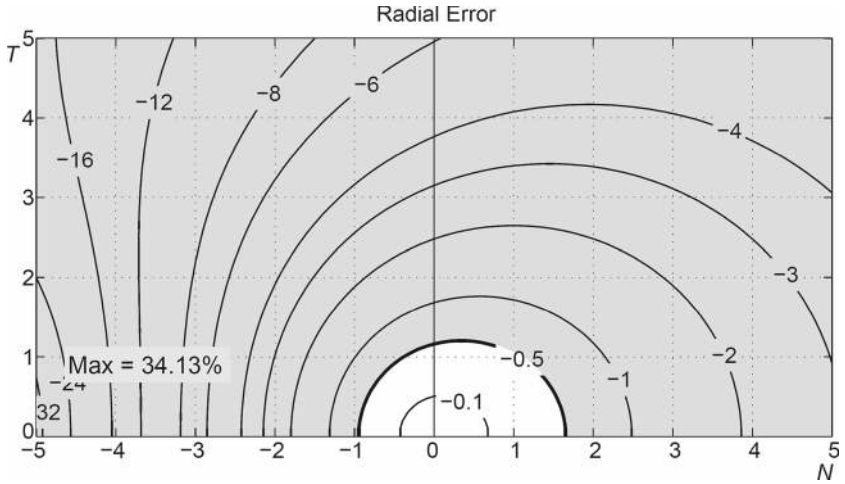

Fig. 26 The radial error for FEX-I, $V = 1$

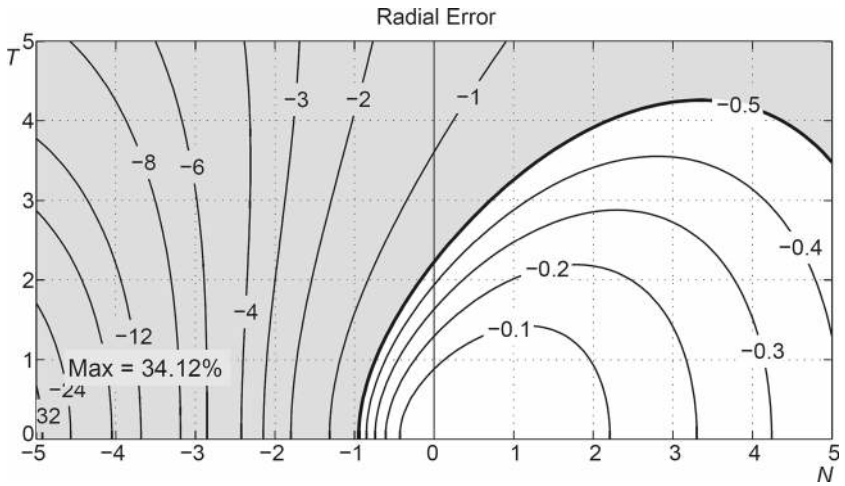

Fig. 27 The radial error for FEX-II, $V = 1$

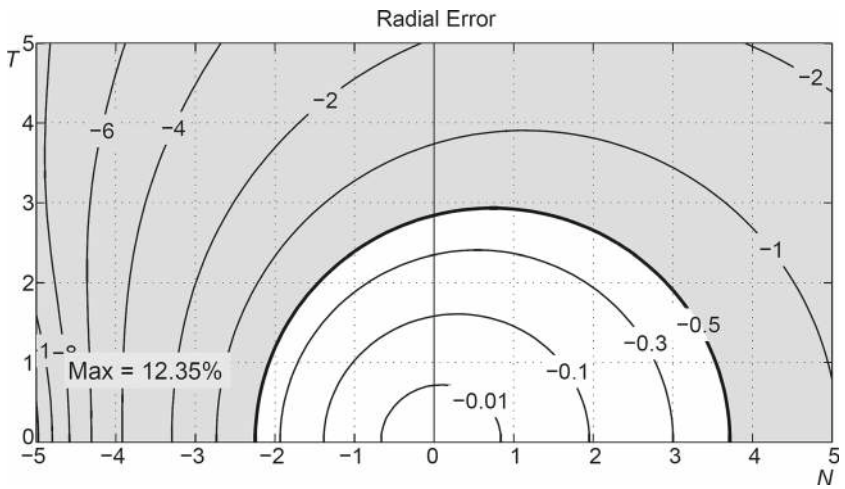

Fig. 28 The radial error for SIM-I, $V = 1$

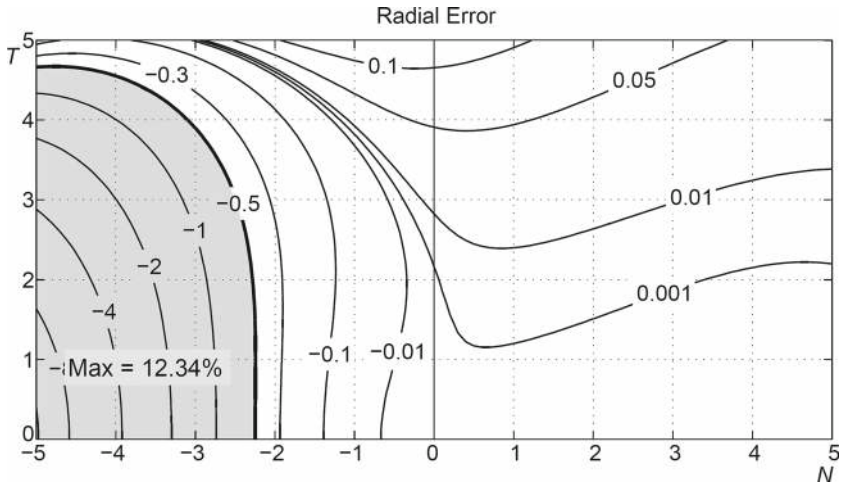

Fig. 29 The radial error for SIM-II, $V = 1$

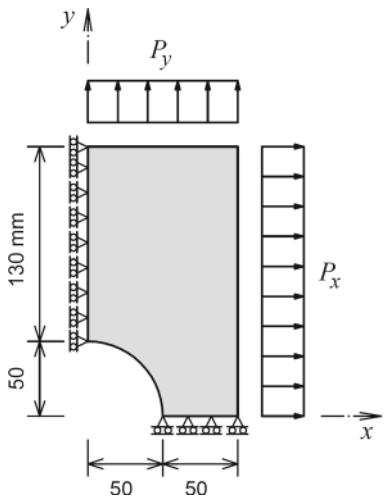

Fig. 30 One-quarter of the strip with circular hole

6.3 Boundary value problems

In this section, two boundary value problems are solved. The goal here is to verify the derived consistent tangent operators and investigate the efficiency of the two presented semi-implicit schemes through comparing their efficiency against the efficiency of the two fully explicit exponential-based integrations when used in a finite element analysis. To meet this purpose, an implicit finite element code is provided, which uses the path-independent strategy and Newton-Raphson solution. The general properties of a kind of high-strength steel are used in these analyses (see [44]):

$$E = 203{,}000\,\text{MPa}, \quad \nu = 0.27, \quad \tau_{y0} = 953\,\text{MPa}, \quad \beta = 0.0693.$$

The hardening properties are given by

$$H_{\text{kin}} = 150{,}000\,\text{MPa}, \quad H_{\text{iso}} = 500.$$

The boundary value problems consist of two rectangular strips with circular and elliptical holes in their centers under the plane strain conditions. The thickness of the strips is assumed to be equal to 1, and the analyses are carried out by applying uniform load control on the direction perpendicular to the sides of the strips symmetrically. As a result, it is obvious that only one quarter of the strips must be analyzed. The geometries of the strips along with the applied loads are shown in Figs. 30 and 31.

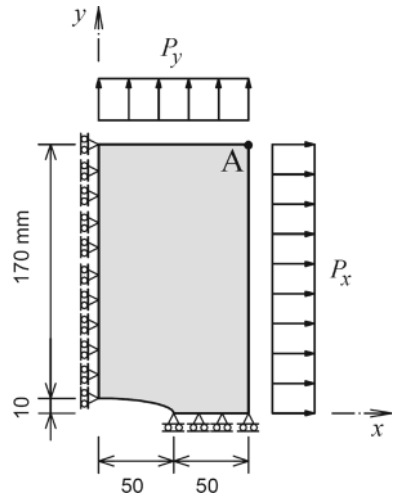

Fig. 31 One-quarter of the strip with elliptical hole

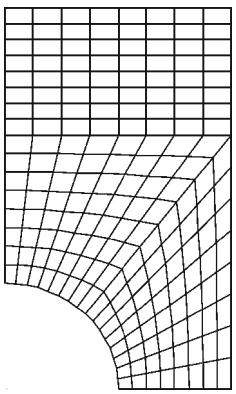

Fig. 32 The finite elements mesh for one-quarter of the strip with circular hole

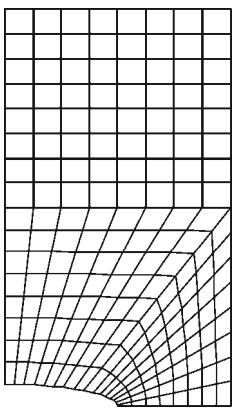

Fig. 33 The finite elements mesh for one-quarter of the strip with elliptical hole

The one quarter of the strips is discretized via 192 4-node isoparametric bilinear quadrilaterals as shown in Figs. 32 and 33. The non-proportional load history is illustrated in Fig. 34. The calculations are carried out by applying the loads in 4 steps per second. Also, the analyses are performed using each stress updating algorithm in question.

First of all, the displacement history of the point A of the strip with elliptical hole is displayed in Fig. 35 using the AC algorithm. To compare the accuracy of the new algorithms (SIM-I and SIM-II) with the

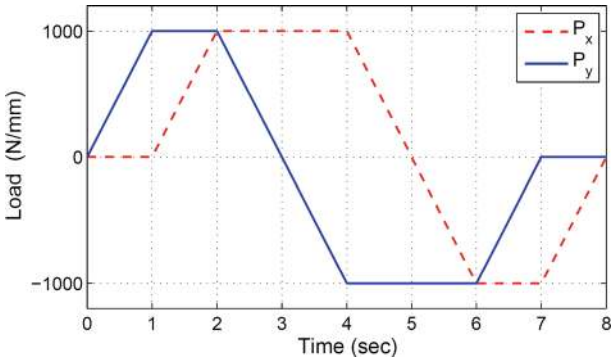

Fig. 34 The history of the biaxial non-proportional loads

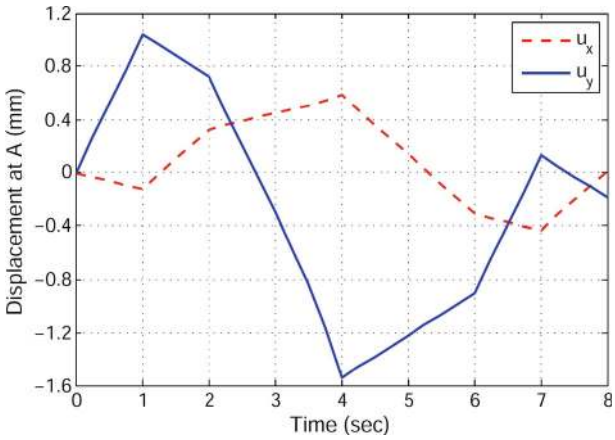

Fig. 35 The history of the displacements for the point A of the strip with elliptical hole

previous ones (FEX-I and FEX-II), the displacement relative error is calculated in each loading increment by the following equation:

$$E_j^{\mathrm{Disp}} = \frac{\left\| \mathbf{u}_j^{\mathrm{E}} - \mathbf{u}_j^{\mathrm{N}} \right\|}{\left\| \mathbf{u}_j^{\mathrm{E}} \right\|}, \qquad \mathbf{u}^{\mathrm{T}} = \left\{ u_1, u_2, \ldots, u_{N_{\mathrm{node}}} \right\}, \qquad u_i = \sqrt{u_{\mathrm{x},i}^2 + u_{\mathrm{y},i}^2}, \tag{85}$$

where the vector $\mathbf{u}_j^{\mathrm{E}}$ denotes the global displacements of the nodes in the jth increment computed by 100 sub-increments using the accurate integration (AC) for stress updating, which is assumed as "reference result". Moreover, $\mathbf{u}_j^{\mathrm{N}}$ is the global displacement vector in the jth increment when one of the aforementioned numerical integrations is used. Considering the strip with elliptical hole, the errors of each fully explicit algorithm with the corresponding semi-implicit one are shown separately in Figs. 36 and 37. The figures illustrate the robustness of the new algorithms, as the accuracies of the SIM-I and SIM-II are much better than the FEX-I and FEX-II schemes.

The deformations of the strips and the elements involved in the plasticity computations in the 4th and 28th loading increments are presented in Figs. 38 and 39. For verifying the consistent tangent operators, the Euclidian norm of the residual forces of the Newton iterations for the 4th and 28th loading increments are presented in Tables 1 and 2, respectively, for the circular and elliptical perforated strips. The results shown in the tables obviously exhibit the quadratic rate of the asymptotic convergence for all schemes.

To test the efficiency of the global solution in a finite element analysis associated with the different stress updating algorithms, the efficiency is defined as the accuracy per computation time and presented by the following relation:

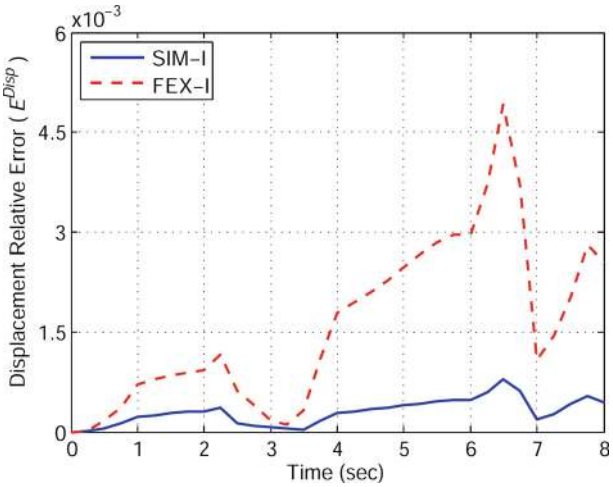

Fig. 36 The displacement relative errors for strip with elliptical hole using the SIM-I and FEX-I algorithms

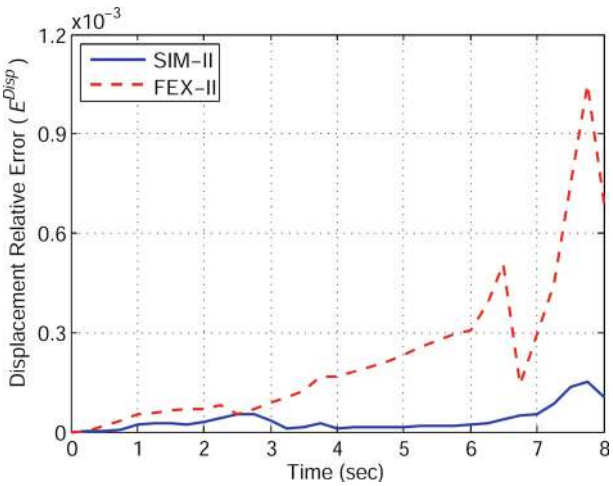

Fig. 37 The displacement relative errors for strip with elliptical hole using the SIM-II and FEX-II algorithms

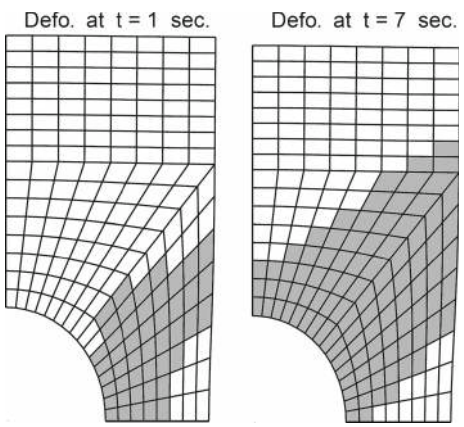

Fig. 38 The deformations and the elements involved in the plasticity computations in the 4th and 28th increments for the strip with circular hole

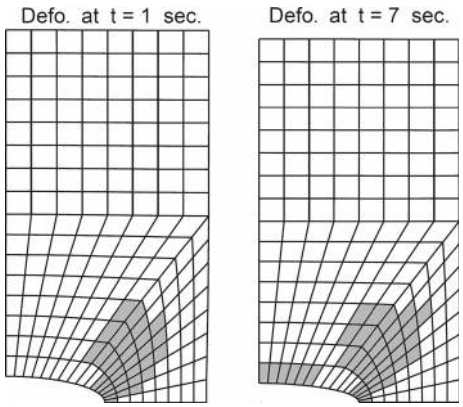

Fig. 39 The deformations and the elements involved in the plasticity computations in 4th and 28th increments for the strip with elliptical hole

Table 1 Residual norms for analysis of strip with circular hole at 4th increment

Iteration	FEX-I	FEX-II	SIM-I	SIM-II	AC
1	$8.5582 \times 10^{+3}$	$8.5582 \times 10^{+3}$	$8.5582 \times 10^{+3}$	$8.5582 \times 10^{+3}$	$8.5582 \times 10^{+3}$
2	$1.7269 \times 10^{+3}$	$1.7261 \times 10^{+3}$	$1.7364 \times 10^{+3}$	$1.7269 \times 10^{+3}$	$1.7264 \times 10^{+3}$
3	$1.0709 \times 10^{+2}$	$1.1236 \times 10^{+2}$	$1.1102 \times 10^{+2}$	$1.1259 \times 10^{+2}$	$1.3528 \times 10^{+2}$
4	$2.4567 \times 10^{+0}$	$1.7388 \times 10^{+0}$	$1.3620 \times 10^{+0}$	$1.7459 \times 10^{+0}$	$4.6159 \times 10^{+0}$
5	2.5234×10^{-2}	3.4805×10^{-2}	1.9720×10^{-2}	3.5040×10^{-2}	1.4178×10^{-1}
6	3.9581×10^{-4}	7.9937×10^{-4}	3.5849×10^{-4}	8.0588×10^{-4}	5.5595×10^{-3}

Table 2 Residual norms for analysis of strip with elliptical hole at 28th increment

Iteration	FEX-I	FEX-II	SIM-I	SIM-II	AC
1	$8.5582 \times 10^{+3}$	$8.5582 \times 10^{+3}$	$8.5582 \times 10^{+3}$	$8.5582 \times 10^{+3}$	$8.5582 \times 10^{+3}$
2	$1.7566 \times 10^{+3}$	$1.6955 \times 10^{+3}$	$1.7097 \times 10^{+3}$	$1.7058 \times 10^{+3}$	$1.9843 \times 10^{+3}$
3	$8.5621 \times 10^{+1}$	$5.2268 \times 10^{+1}$	$6.3067 \times 10^{+1}$	$5.5454 \times 10^{+1}$	$3.1007 \times 10^{+2}$
4	$1.0203 \times 10^{+0}$	7.7905×10^{-1}	8.5586×10^{-1}	6.8710×10^{-1}	$1.6403 \times 10^{+1}$
5	1.8349×10^{-2}	1.3390×10^{-2}	1.4684×10^{-2}	1.2905×10^{-2}	$3.0196 \times 10^{+0}$
6	–	–	–	–	1.5874×10^{-1}
7	–	–	–	–	4.3879×10^{-2}

$$\eta = \frac{1}{T_{\mathrm{CPU}} \times E_{\mathrm{T}}}, \tag{86}$$

where T_{CPU} denotes the total CPU time recorded in the analysis, and the accuracy has been defined as $1/E_{\mathrm{T}}$, in which E_{T} is the total error of the nodes' displacements computed by:

$$E_{\mathrm{T}} = \sum_{j=1}^{N_{\mathrm{incr}}} \frac{\left\| \mathbf{u}_j^{\mathrm{E}} - \mathbf{u}_j^{\mathrm{N}} \right\|}{\left\| \mathbf{u}_j^{\mathrm{E}} \right\|}. \tag{87}$$

In the above equation, N_{incr} represents the total number of loading increments, and the vectors $\mathbf{u}_j^{\mathrm{E}}$ and $\mathbf{u}_j^{\mathrm{N}}$ were defined previously. Having a comprehensive test, the classical Forward Euler (FE) and Backward Euler (BE) schemes are employed. The results are presented in Tables 3 and 4, respectively, for the strips with circular and elliptical holes. Based upon the findings of these tables, it is deduced that the SIM-II scheme presents a superior efficiency compared to others. Furthermore, the FE scheme has the worst effectiveness. Moreover, the FEX-I shows the lowest efficiency among the exponential-based schemes as it is placed lower than BE. However, the improved form of FEX-I, i.e. SIM-I is upgraded very well since its efficiency is about 5 times higher than the efficiency of FEX-I. In addition, it is worth mentioning that although the efficiency of SIM-I is less than the efficiency of FEX-II, SIM-I has second-order accuracy, which is a benefit over the explicit FEX-II

Table 3 Efficiency for the analysis of strip with circular hole when different updating stress schemes are used

Scheme	T_{CPU}(s)	E_{T}	η	$\eta_{\mathrm{n}} = \eta/\eta_{\mathrm{FE}}$
FE	92.34	0.0914	0.1185	1
BE	82.55	0.0296	0.4094	3.46
FEX-I	104.54	0.0317	0.3017	2.55
FEX-II	101.17	0.0042	2.3520	19.85
SIM-I	109.74	0.0052	1.7420	14.71
SIM-II	109.17	0.0005	19.1729	161.84

Table 4 Efficiency for the analysis of strip with elliptical hole when different updating stress schemes are used

Scheme	T_{CPU}(s)	E_{T}	η	$\eta_{\mathrm{n}} = \eta/\eta_{\mathrm{FE}}$
FE	67.02	0.0160	0.9328	1
BE	59.66	0.0094	1.7909	1.92
FEX-I	71.58	0.0127	1.1036	1.18
FEX-II	73.45	0.0019	7.1915	7.71
SIM-I	73.19	0.0024	5.7433	6.16
SIM-II	78.98	0.0003	43.8239	46.98

scheme. Therefore, it is evident that where the results become more accurate, the efficiency of the analysis grows more when SIM-I is used instead of FEX-II.

7 Conclusions

The Drucker-Prager yield condition was considered along with the kinematic and isotropic hardenings. Previously, two fully explicit exponential-based integrations were proposed (FEX-I and FEX-II) in Reference [30]. In order to improve the aforementioned schemes, they were converted to two semi-implicit integration algorithms (SIM-I and SIM-II) in Sects. 3.3 and 4.3. In addition, the consistent tangent operators, which are necessary for the implicit finite element codes, were derived for all the fully explicit and semi-implicit schemes in Sects. 3.2, 3.4, 4.2 and 4.4. Subsequently, the consistent tangent operator for an accurate integration was obtained in Sect. 5.2.

In order to evaluate the accuracy, precision order and efficiency of the new semi-implicit tactics, the numerical investigations consisting of the strain load histories, iso-error maps and boundary value problems were taken into account. The findings illustrated the superior accuracy of the new semi-implicit schemes over the fully explicit ones. Furthermore, it was shown that the semi-implicit methods have second-order accuracy compared to the first-order precision of the fully explicit schemes. The results of the boundary value problems demonstrated that the efficiency of the finite element analyses, when the semi-implicit stress updating algorithms (SIM-I and SIM-II) are used, is much higher than that of those with the fully explicit algorithms (FEX-I and FEX-II). Finally, the correctness of the derived consistent tangent operators was proven, as well.

Appendix A: Computing the scalar parameter α

The scalar parameter α could be easily computed solving the algebraic equation $F(\mathbf{s}'_n + 2G(\alpha\Delta\mathbf{e}), p'_n + K\alpha\Delta\varepsilon_{\mathrm{v}}) = 0$:

$$\alpha = \frac{\sqrt{B^2 - 4AC} - B}{2A}, \tag{A1}$$

where A, B and C are given by:

$$\begin{aligned} A &= \|2G\Delta\mathbf{e}\|^2 - 2(\beta K\Delta\varepsilon_{\mathrm{v}})^2, \\ B &= 4G\Delta\mathbf{e}^{\mathrm{T}}\mathbf{s}'_n + 4\beta K(\tau_{\mathrm{y},n} - \beta p'_n)\Delta\varepsilon_{\mathrm{v}}, \\ C &= \left\|\mathbf{s}'_n\right\|^2 - 2(\tau_{\mathrm{y},n} - \beta p'_n)^2. \end{aligned} \tag{A2}$$

Appendix B: Derivatives addressed in the consistent tangent operator of the *fully explicit* exponential-based integration with *one* integrating factor

The derivatives appearing in Eqs. (33) and (34) are presented in the following. First, taking the derivative of $\mathbf{X}^{\mathrm{s}}_{n+\alpha}$ and $X^{\mathrm{R}}_{n+\alpha}$ with respect to $\mathbf{e}_{n+1}$ determines the following equations:

$$\begin{aligned}
\frac{\partial \mathbf{X}^{\mathrm{s}}_{n+\alpha}}{\partial \mathbf{e}_{n+1}} &= 2G\alpha X^{0}_{n+\alpha}\mathbb{I} + 2GX^{0}_{n+\alpha}\Delta\mathbf{e}\left(\frac{\partial \alpha}{\partial \mathbf{e}_{n+1}}\right)^{\mathrm{T}},\\
\frac{\partial X^{\mathrm{R}}_{n+\alpha}}{\partial \mathbf{e}_{n+1}} &= -\sqrt{2}\beta K X^{0}_{n+\alpha}\Delta\varepsilon_{\mathrm{v}}\frac{\partial \alpha}{\partial \mathbf{e}_{n+1}},
\end{aligned} \tag{B1}$$

where $\partial\alpha/\partial\mathbf{e}_{n+1}$ is given as

$$\frac{\partial \alpha}{\partial \mathbf{e}_{n+1}} = \frac{4G^2}{A^2}\left(-\frac{2AC}{\sqrt{B^2-4AC}} - \sqrt{B^2-4AC} + B\right)\Delta\mathbf{e} + \frac{2G}{A}\left(\frac{B}{\sqrt{B^2-4AC}} - 1\right)\mathbf{s}'_{n}. \tag{B2}$$

In addition, the derivatives of the parameters a, b, c and d can be expressed by:

$$\begin{aligned}
\frac{\partial a_{n+\alpha}}{\partial \mathbf{e}_{n+1}} &= \frac{2G}{R_{n+\alpha}}\left[-\|\Delta\mathbf{e}\|\frac{\partial \alpha}{\partial \mathbf{e}} + (1-\alpha)\frac{\partial \|\Delta\mathbf{e}\|}{\partial \mathbf{e}} - \frac{(1-\alpha)\|\Delta\mathbf{e}\|}{R_{n+\alpha}}\frac{\partial R_{n+\alpha}}{\partial \mathbf{e}}\right]b_{n+\alpha},\\
\frac{\partial b_{n+\alpha}}{\partial \mathbf{e}_{n+1}} &= \frac{a_{n+\alpha}}{b_{n+\alpha}}\frac{\partial a_{n+\alpha}}{\partial \mathbf{e}_{n+1}},\\
\frac{\partial c_{n+\alpha}}{\partial \mathbf{e}_{n+1}} &= \frac{1}{Q_{n+\alpha}}\frac{\partial R_{n+\alpha}}{\partial \mathbf{e}} - \frac{R_{n+\alpha}}{Q_{n+\alpha}}\frac{\partial Q_{n+\alpha}}{\partial \mathbf{e}},\\
\frac{\partial d_{n+\alpha}}{\partial \mathbf{e}_{n+1}} &= \frac{R_{n+\alpha}}{Q_{n+\alpha}}\frac{\partial V_{n+\alpha}}{\partial \mathbf{e}} + \frac{V_{n+\alpha}}{Q_{n+\alpha}}\frac{\partial R_{n+\alpha}}{\partial \mathbf{e}} - \frac{V_{n+\alpha}R_{n+\alpha}}{Q^2_{n+\alpha}}\frac{\partial Q_{n+\alpha}}{\partial \mathbf{e}},
\end{aligned} \tag{B3}$$

introducing

$$\begin{aligned}
\frac{\partial Q_{n+\alpha}}{\partial \mathbf{e}_{n+1}} &= \frac{2(\bar{G}+K\beta^2)R_{n+\alpha}}{\bar{G}}\frac{\partial R_{n+\alpha}}{\partial \mathbf{e}} + \frac{H_{\mathrm{iso}}}{\sqrt{2}\bar{G}}\frac{\partial R_{n+\alpha}}{\partial \mathbf{e}},\\
\frac{\partial R_{n+\alpha}}{\partial \mathbf{e}_{n+1}} &= -\sqrt{2}\beta K\Delta\varepsilon_{\mathrm{v}}\frac{\partial \alpha}{\partial \mathbf{e}_{n+1}},\\
\frac{\partial V_{n+\alpha}}{\partial \mathbf{e}_{n+1}} &= -\frac{\beta K\Delta\varepsilon_{\mathrm{v}}}{\sqrt{2}G\|\Delta\mathbf{e}\|^2}\Delta\hat{\mathbf{e}}.
\end{aligned} \tag{B4}$$

Appendix C: Derivatives addressed in the consistent tangent operator of the *semi-implicit* exponential-based integration with *one* integrating factor

As was mentioned in Sect. 3.4, the derivatives of a, b, c and d, which have subscript $n+r(1-\alpha)$, are needed. To meet this objective, one could use the relations presented in Eqs. (B3) and (B4) with the subscript of $n+r(1-\alpha)$ instead of $n+\alpha$ and with

$$\frac{\partial R_{n+r(1-\alpha)}}{\partial \mathbf{e}} = \frac{1}{A_2}\frac{\partial A_1}{\partial \mathbf{e}} - \frac{A_1}{A_2^2}\frac{\partial A_2}{\partial \mathbf{e}}, \tag{C1}$$

where

$$\begin{aligned}
A_1 &= \bar{b}_{n+\alpha}\Delta\hat{\mathbf{e}}^{\mathrm{T}}\mathbf{s}'_{n+\alpha} + \bar{a}_{n+\alpha}R_{n+\alpha},\\
A_2 &= [c_{n+\alpha}\bar{b}_{n+\alpha} + (\bar{a}_{n+\alpha}-1)d_{n+\alpha}]\Delta\hat{\mathbf{e}}^{\mathrm{T}}\mathbf{s}'_{n+\alpha} + [d_{n+\alpha}\bar{b}_{n+\alpha} + (\bar{a}_{n+\alpha}-1)c_{n+\alpha}]R_{n+\alpha} + 1
\end{aligned} \tag{C2}$$

and,

$$\begin{aligned}
\frac{\partial A_1}{\partial \mathbf{e}_{n+1}} &= \left(\Delta\hat{\mathbf{e}}^{\mathrm{T}}\mathbf{s}'\right)\frac{\partial \bar{b}}{\partial \mathbf{e}} + \bar{b}\frac{\partial \Delta\hat{\mathbf{e}}}{\partial \mathbf{e}}\mathbf{s}' + \bar{b}\frac{\partial \mathbf{s}'}{\partial \mathbf{e}}\Delta\hat{\mathbf{e}} + R\frac{\partial \bar{a}}{\partial \mathbf{e}} + a\frac{\partial R}{\partial \mathbf{e}},\\
\frac{\partial A_2}{\partial \mathbf{e}_{n+1}} &= \left[\bar{b}\frac{\partial c}{\partial \mathbf{e}} + c\frac{\partial \bar{b}}{\partial \mathbf{e}} + (\bar{a}-1)\frac{\partial d}{\partial \mathbf{e}} + d\frac{\partial \bar{a}}{\partial \mathbf{e}}\right]\Delta\hat{\mathbf{e}}^{\mathrm{T}}\mathbf{s}' + \left[c\cdot\bar{b} + (\bar{a}-1)d\right]\left(\frac{\partial \Delta\hat{\mathbf{e}}}{\partial \mathbf{e}}\mathbf{s}' + \frac{\partial \mathbf{s}'}{\partial \mathbf{e}}\Delta\hat{\mathbf{e}}\right)\\
&\quad + \left[d\frac{\partial \bar{b}}{\partial \mathbf{e}} + \bar{b}\frac{\partial d}{\partial \mathbf{e}} + (\bar{a}-1)\frac{\partial c}{\partial \mathbf{e}} + c\frac{\partial \bar{a}}{\partial \mathbf{e}}\right]R + \left[d\cdot b + (a-1)c\right]\frac{\partial R}{\partial \mathbf{e}}.
\end{aligned} \tag{C3}$$

In these equations all the parameters $\bar{a}$, $\bar{b}$, c, d and R get the subscript of $n+\alpha$; the derivatives of c, d and R with respect to $\mathbf{e}_{n+1}$ were presented in the former sections, and for $\partial\bar{a}_{n+\alpha}/\partial\mathbf{e}_{n+1}$ and $\partial\bar{b}_{n+\alpha}/\partial\mathbf{e}_{n+1}$, one obtains the following relations:

$$\begin{aligned}
\frac{\partial \bar{a}_{n+\alpha}}{\partial \mathbf{e}_{n+1}} &= \frac{2Gr}{R_{n+\alpha}}\left[-\left\|\Delta\mathbf{e}\right\|\frac{\partial \alpha}{\partial \mathbf{e}} + (1-\alpha)\frac{\partial \left\|\Delta\mathbf{e}\right\|}{\partial \mathbf{e}} - \frac{1}{R_{n+\alpha}}(1-\alpha)\left\|\Delta\mathbf{e}\right\|\frac{\partial R_{n+\alpha}}{\partial \mathbf{e}}\right]\bar{b}_{n+\alpha},\\
\frac{\partial \bar{b}_{n+\alpha}}{\partial \mathbf{e}_{n+1}} &= \frac{\bar{a}_{n+\alpha}}{\bar{b}_{n+\alpha}}\frac{\partial \bar{a}_{n+\alpha}}{\partial \mathbf{e}_{n+1}}.
\end{aligned} \tag{C4}$$

Appendix D: Derivatives addressed in the consistent tangent operator of the *fully explicit* exponential-based integration with *two* integrating factors

To compute the consistent tangent operator corresponding to the fully explicit exponential-based integration with two integrating factors, one should take the derivatives of $\mathbf{X}^{\mathrm{s}}_{a,n+\alpha}$, $X^0_{a,n+\alpha}$, $X^1_{b,n+\alpha}$ and $X^0_{b,n+\alpha}$ in the following way:

$$\begin{aligned}
\frac{\partial \mathbf{X}^{\mathrm{s}}_{a,n+\alpha}}{\partial \mathbf{e}_{n+1}} &= X^0_{n+\alpha}\frac{\partial \mathbf{s}'_{n+\alpha}}{\partial \mathbf{e}_{n+1}},\\
\frac{\partial X^0_{a,n+\alpha}}{\partial \mathbf{e}_{n+1}} &= X^0_{n+\alpha}\frac{\partial R_{n+\alpha}}{\partial \mathbf{e}_{n+1}},\\
\frac{\partial X^1_{b,n+\alpha}}{\partial \mathbf{e}_{n+1}} &= -\beta K\Delta\varepsilon_{\mathrm{v}}x^0_{n+\alpha}\frac{\partial \alpha}{\partial \mathbf{e}},\\
\frac{\partial X^0_{b,n+\alpha}}{\partial \mathbf{e}_{n+1}} &= x^0_{n+\alpha}\frac{\partial R_{n+\alpha}}{\partial \mathbf{e}},
\end{aligned} \tag{D1}$$

where

$$\frac{\partial \mathbf{s}'_{n+\alpha}}{\partial \mathbf{e}_{n+1}} = 2G\alpha\mathbb{I} + 2G\Delta\mathbf{e}\left(\frac{\partial \alpha}{\partial \mathbf{e}}\right)^{\mathrm{T}}. \tag{D2}$$

Moreover, $\partial u_{n+\alpha}/\partial\mathbf{e}_{n+1}$ and $\partial v_{n+\alpha}/\partial\mathbf{e}_{n+1}$ could be derived as

$$\begin{aligned}
\frac{\partial u_{n+\alpha}}{\partial \mathbf{e}_{n+1}} &= \sinh\left(g_{n+\alpha}\right)\frac{\partial g_{n+\alpha}}{\partial \mathbf{e}},\\
\frac{\partial v_{n+\alpha}}{\partial \mathbf{e}_{n+1}} &= \cosh\left(g_{n+\alpha}\right)\frac{\partial g_{n+\alpha}}{\partial \mathbf{e}},
\end{aligned} \tag{D3}$$

where $\partial g_{n+\alpha}/\partial\mathbf{e}$ appearing in the above equations can be expressed by:

$$\begin{aligned}
\frac{\partial g_{n+\alpha}}{\partial \mathbf{e}_{n+1}} &= -\frac{\sqrt{2}g}{R}\frac{\partial R}{\partial \mathbf{e}} + \frac{\beta K(1-\alpha)\Delta\varepsilon_{\mathrm{v}}}{R}\frac{\partial \bar{Q}}{\partial \mathbf{e}} - \frac{\beta K\Delta\varepsilon_{\mathrm{v}}(\bar{Q}-1)}{R}\frac{\partial \alpha}{\partial \mathbf{e}} + \frac{\sqrt{2}G(1-\alpha)(\mathbf{n}^{\mathrm{T}}\Delta\mathbf{e})}{R}\frac{\partial \bar{Q}}{\partial \mathbf{e}}\\
&\quad - \frac{\sqrt{2}G\bar{Q}(\mathbf{n}^{\mathrm{T}}\Delta\mathbf{e})}{R}\frac{\partial \alpha}{\partial \mathbf{e}} + \frac{\sqrt{2}G\bar{Q}(1-\alpha)}{R}\frac{\partial \mathbf{n}}{\partial \mathbf{e}}\Delta\mathbf{e} + \frac{\sqrt{2}G\bar{Q}(1-\alpha)}{R}\mathbf{n}.
\end{aligned} \tag{D4}$$

In the last equation, all variables R, $\bar{Q}$ and $\mathbf{n}$ get a subscript of $n+\alpha$, and the derivatives $\partial \bar{Q}_{n+\alpha}/\partial \mathbf{e}$ and $\partial \mathbf{n}_{n+\alpha}/\partial \mathbf{e}$ hold as:

$$\begin{aligned}\frac{\partial \bar{Q}_{n+\alpha}}{\partial \mathbf{e}_{n+1}} &= -\frac{\sqrt{2}H_{\text{iso}}}{[\sqrt{2}(\bar{G}+\bar{K}\beta^2)R+H_{\text{iso}}]^2}\left[\sqrt{2}(\bar{G}+\bar{K}\beta^2)\frac{\partial R}{\partial \mathbf{e}}\right],\\ \frac{\partial \mathbf{n}_{n+\alpha}}{\partial \mathbf{e}_{n+1}} &= \frac{1}{X^0}\frac{\partial \mathbf{X}^{\text{s}}_a}{\partial \mathbf{e}} - \frac{\mathbf{X}^{\text{s}}_a}{(X^0)^2}\left(\frac{\partial X^0}{\partial \mathbf{e}}\right)^{\text{T}},\end{aligned} \tag{D5}$$

where R, X^0 and $\mathbf{X}^{\text{s}}_a$ get a subscript of $n+\alpha$.

Appendix E: Derivatives addressed in the consistent tangent operator of the *semi-implicit* exponential-based integration with *two* integrating factors

How to determine the derivatives $\partial a_{n+r(1-\alpha)}/\partial \mathbf{e}_{n+1}$ and $\partial b_{n+r(1-\alpha)}/\partial \mathbf{e}_{n+1}$, which appear in the consistent tangent operator of the semi-implicit integration with two factors, was addressed in Appendix C. Also, $\partial u_{n+r(1-\alpha)}/\partial \mathbf{e}_{n+1}$, $\partial v_{n+r(1-\alpha)}/\partial \mathbf{e}_{n+1}$ and $\partial g_{n+r(1-\alpha)}/\partial \mathbf{e}$ could be straightforwardly obtained by replacing the subscript $n+\alpha$ with $n+r(1-\alpha)$ for all variables of Eqs. (D3)–(D5). In addition, the following derivatives are needed:

$$\frac{\partial R_{n+r(1-\alpha)}}{\partial \mathbf{e}_{n+1}} = \frac{1}{X^0_{n+r(1-\alpha)}}\frac{\partial X^0_{a,n+r(1-\alpha)}}{\partial \mathbf{e}} - \frac{X^0_{a,n+r(1-\alpha)}}{\left(X^0_{n+r(1-\alpha)}\right)^2}\frac{\partial X^0_{n+r(1-\alpha)}}{\partial \mathbf{e}}, \tag{E1}$$

$$\frac{\partial X^0_{n+r(1-\alpha)}}{\partial \mathbf{e}_{n+1}} = \frac{\bar{G}}{\bar{K}\beta^2+\bar{G}}\left(\frac{X^0_{a,n+r(1-\alpha)}}{X^0_{b,n+r(1-\alpha)}}\right)^{\frac{-\bar{K}\beta^2}{\bar{K}\beta^2+\bar{G}}}\left[\frac{1}{X^0_{b,n+r(1-\alpha)}}\frac{\partial X^0_{a,n+r(1-\alpha)}}{\partial \mathbf{e}} - \frac{X^0_{a,n+r(1-\alpha)}}{\left(X^0_{b,n+r(1-\alpha)}\right)^2}\frac{\partial X^0_{b,n+r(1-\alpha)}}{\partial \mathbf{e}}\right], \tag{E2}$$

where the derivative $\partial X^0_{a,n+r(1-\alpha)}/\partial \mathbf{e}_{n+1}$ has the same relationship as Eq. (58), but $\partial X^0_{b,n+r(1-\alpha)}/\partial \mathbf{e}_{n+1}$ could be given as:

$$\frac{\partial X^0_{\text{b},n+1}}{\partial \mathbf{e}_{n+1}} = \sqrt{2}X^1_{\text{b},n+\alpha}\frac{\partial \bar{v}_{n+\alpha}}{\partial \mathbf{e}_{n+1}} + \sqrt{2}\bar{v}_{n+\alpha}\frac{\partial X^1_{\text{b},n+\alpha}}{\partial \mathbf{e}_{n+1}} + X^0_{\text{b},n+\alpha}\frac{\partial \bar{u}_{n+\alpha}}{\partial \mathbf{e}_{n+1}} + \bar{u}_{n+\alpha}\frac{\partial X^0_{\text{b},n+\alpha}}{\partial \mathbf{e}_{n+1}}, \tag{E3}$$

in which

$$\begin{aligned}\frac{\partial \bar{u}_{n+\alpha}}{\partial \mathbf{e}_{n+1}} &= r\sinh(rg_{n+\alpha})\frac{\partial g_{n+\alpha}}{\partial \mathbf{e}},\\ \frac{\partial \bar{v}_{n+\alpha}}{\partial \mathbf{e}_{n+1}} &= r\cosh(rg_{n+\alpha})\frac{\partial g_{n+\alpha}}{\partial \mathbf{e}}.\end{aligned} \tag{E4}$$

Appendix F: Derivatives addressed in the consistent tangent operator of the *accurate* integration

In what follows, all the derivatives mentioned in Sect. 5.2 are given as:

$$\begin{aligned}\frac{\partial f_1}{\partial y_1} &= \frac{2\bar{G}(\sqrt{2}G||\dot{\mathbf{e}}||\cos y_2+\beta K\dot{\varepsilon}_{\text{v}})}{H_{\text{iso}}+\sqrt{2}(\bar{G}+\bar{K}\beta^2)y_1}\left(\frac{\sqrt{2}(\bar{G}+\bar{K}\beta^2)y_1}{H_{\text{iso}}+\sqrt{2}(\bar{G}+\bar{K}\beta^2)y_1}-1\right),\\ \frac{\partial f_1}{\partial y_2} &= -2G||\dot{\mathbf{e}}||\sin y_2 + \frac{2\sqrt{2}G\bar{G}||\dot{\mathbf{e}}||y_1\sin y_2}{H_{\text{iso}}+\sqrt{2}(\bar{G}+\bar{K}\beta^2)y_1},\\ \frac{\partial f_2}{\partial y_1} &= \frac{2G||\dot{\mathbf{e}}||\sin y_2}{y_1^2},\\ \frac{\partial f_2}{\partial y_2} &= -\frac{2G||\dot{\mathbf{e}}||\cos y_2}{y_1},\end{aligned} \tag{F1}$$

and

$$\begin{aligned}
\frac{\partial \xi}{\partial \mathbf{e}_{n+1}} &= \frac{\sin\psi_{n+1}}{R_{n+\alpha}\sin^2\psi_{n+\alpha}}\frac{\partial R_{n+1}}{\partial \mathbf{e}_{n+1}} + \frac{R_{n+1}\cos\psi_{n+1}}{R_{n+\alpha}\sin\psi_{n+\alpha}}\frac{\partial \psi_{n+1}}{\partial \mathbf{e}_{n+1}} - \frac{R_{n+1}\sin\psi_{n+1}}{R_{n+\alpha}^2\sin\psi_{n+\alpha}}\frac{\partial R_{n+\alpha}}{\partial \mathbf{e}_{n+1}} \\
&\quad - \frac{R_{n+1}\sin\psi_{n+1}\cos\psi_{n+\alpha}}{R_{n+\alpha}\sin^2\psi_{n+\alpha}}\frac{\partial \psi_{n+\alpha}}{\partial \mathbf{e}_{n+1}}, \\
\frac{\partial \zeta}{\partial \mathbf{e}_{n+1}} &= \frac{\sin(\psi_{n+\alpha}-\psi_{n+1})}{\left\|\Delta \mathbf{s}'^{\mathrm{TR}}\right\|\sin\psi_{n+\alpha}}\frac{\partial R_{n+1}}{\partial \mathbf{e}_{n+1}} + \frac{R_{n+1}\cos(\psi_{n+\alpha}-\psi_{n+1})}{\left\|\Delta \mathbf{s}'^{\mathrm{TR}}\right\|\sin\psi_{n+\alpha}}\left(\frac{\partial \psi_{n+\alpha}}{\partial \mathbf{e}_{n+1}} - \frac{\partial \psi_{n+1}}{\partial \mathbf{e}_{n+1}}\right) \\
&\quad - \frac{R_{n+1}\sin(\psi_{n+\alpha}-\psi_{n+1})}{\left\|\Delta \mathbf{s}'^{\mathrm{TR}}\right\|^2\sin\psi_{n+\alpha}}\frac{\partial \left\|\Delta \mathbf{s}'^{\mathrm{TR}}\right\|}{\partial \mathbf{e}_{n+1}} - \frac{R_{n+1}\sin(\psi_{n+\alpha}-\psi_{n+1})\cos\psi_{n+\alpha}}{\left\|\Delta \mathbf{s}'^{\mathrm{TR}}\right\|\sin^2\psi_{n+\alpha}}\frac{\partial \psi_{n+\alpha}}{\partial \mathbf{e}_{n+1}},
\end{aligned} \tag{F2}$$

$$\begin{aligned}
\frac{\partial \left\|\Delta \mathbf{s}'^{\mathrm{TR}}\right\|}{\partial \mathbf{e}_{n+1}} &= \frac{\partial \Delta \mathbf{s}'^{\mathrm{TR}}}{\partial \mathbf{e}_{n+1}}\frac{\Delta \mathbf{s}'^{\mathrm{TR}}}{\left\|\Delta \mathbf{s}'^{\mathrm{TR}}\right\|}, \\
\frac{\partial \Delta \mathbf{s}'^{\mathrm{TR}}}{\partial \mathbf{e}_{n+1}} &= 2G(1-\alpha)\mathbb{I} - 2G\Delta \mathbf{e}\left(\frac{\partial \alpha}{\partial \mathbf{e}}\right)^{\mathrm{T}}.
\end{aligned} \tag{F3}$$

References

1. Wilkins, M.L.: Calculation of elastic-plastic flow. In: Methods in Computational Physics, vol.3. Academic Press, New York (1964)
2. Krieg, R.D., Krieg, D.B.: Accuracies of numerical solution methods for the elastic-perfectly plastic model. J. Press. Vessel Tech. Trans. ASME **99**, 510–515 (1977)
3. Nagtegaal, J.C.: On the implementation of inelastic constitutive equations with special reference to large deformation problems. Comput. Methods Appl. Mech. Eng **33**, 469–484 (1982)
4. Simo, J.C., Taylor, R.L.: Consistent tangent operators for rate-independent elasto-plasticity. Comput. Methods Appl. Mech. Eng. **48**, 101–118 (1985)
5. Dodds, R.H.: Numerical techniques for plasticity computations in finite element analysis. Comput. Struct. **26**(5), 767–779 (1987)
6. Ortiz, M., Popov, E.P.: Accuracy and stability of integration algorithms for elasto-plastic constitutive relations. Int. J. Numer. Methods Eng. **21**, 1561–1576 (1985)
7. Simo, J.C., Taylor, R.L.: A return mapping algorithm for plane stress elasto-plasticity. Int. J. Numer. Methods Eng. **22**, 649–670 (1986)
8. Sloan, S.W., Booker, J.R.: Integration of Tresca and Mohr-Coulomb constitutive relations in plane strain elasto-plasticity. Int. J. Numer. Methods Eng. **33**, 163–196 (1992)
9. Potts, D.M., Ganendra, D.: An evaluation of substepping and implicit stress point algorithms. Comput. Methods Appl. Mech. Eng. **119**, 341–54 (1994)
10. Sloan, S.W., Abbo, A.J., Sheng, D.: Refined explicit integration of elasto-plastic models with automatic error control. Eng. Comput. **18**(1/2), 121–154 (2001)
11. Solowski, W.T., Gallipoli, D.: Explicit integration with error control for the Barcelona basic model. Part II: algorithm efficiency and accuracy. Comput. Geotech. **37**, 68–81 (2010)
12. Loret, B., Prevost, J.H.: Accurate numerical solutions for Drucker-Prager elastic-plastic models. Comput. Methods Appl. Mech. Eng. **54**, 259–277 (1986)
13. Ristinmaa, M., Tryding, J.: Exact integration of constitutive equations in elasto-plasticity. Int. J. Numer. Methods Eng. **36**, 2525–2544 (1993)
14. Wei, Z., Perić, D., Owen, D.R.J.: Consistent linearization for the exact stress update of Prandtl-Reuss non-hardening elasto-plastic models. Int. J. Numer. Methods Eng. **39**, 1219–1235 (1996)
15. Wallin, M., Ristinmaa, M.: Accurate stress updating algorithm based on constant strain rate assumption. Comput. Methods Appl. Mech. Eng. **190**, 5583–5601 (2001)
16. Wallin, M., Ristinmaa, M.: An alternative method for the integration of continuum damage evolution laws. Comput. Mech. **41**, 347–359 (2008)
17. Szabó, L.: A semi-analytical integration method for J2 flow theory of plasticity with linear isotropic hardening. Comput. Methods Appl. Mech. Eng. **198**, 2151–2166 (2009)
18. Kossa, A., Szabó, L.: Exact integration of the von Mises elasto-plasticity model with combined linear isotropic-kinematic hardening. Int. J. Plast **25**, 1083–1106 (2009)
19. Rezaiee-Pajand, M., Sharifian, M.: A novel formulation for integrating nonlinear kinematic hardening Drucker-Prager's yield condition. Eur. J. Mech. A Solids **31**, 163–178 (2012)

20. Auricchio, F., Beirãoda Veiga, F.: On a new integration scheme for von-Mises plasticity with linear hardening. Int. J. Numer. Methods Eng. **56**, 1375–1396 (2003)
21. Hong, H.-K., Liu, C.-S.: Internal symmetry in the constitutive model of perfect elasto-plasticity. Int. J. Non-Linear Mech. **35**, 447–466 (2000)
22. Hong, H.-K., Liu, C.-S.: Lorentz group on Minkowski spacetime for construction of the two basic principles of plasticity. Int. J. Non-Linear Mech. **36**, 679–686 (2001)
23. Liu, C.-S.: Internal Symmetry groups for the Drucker-Prager material model of plasticity and numerical integrating methods. Int. J. Solids Struct. **41**, 3771–3791 (2004)
24. Artioli, E., Auricchio, F., Beirãoda Veiga, L.: Integration schemes for von-Mises plasticity models based on exponential maps: numerical investigations and theoretical considerations. Int. J. Numer. Methods Eng. **64**, 1133–1165 (2005)
25. Artioli, E., Auricchio, F., Beirãoda Veiga, L.: A novel 'optimal' exponential-based integration algorithm for von-Mises plasticity with linear hardening: Theoretical analysis on yield consistency, accuracy, convergence and numerical investigations. Int. J. Numer. Methods Eng. **67**(4), 449–498 (2006)
26. Artioli, E., Auricchio, F., Beirãoda Veiga, L.: Second-order accurate integration algorithms for von-Mises plasticity with a nonlinear kinematic hardening mechanism. Comput. Methods Appl. Mech. Eng. **196**, 1827–1846 (2007)
27. Rezaiee-Pajand, M., Nasirai, C.: Accurate integration scheme for von-Mises plasticity with mixed-hardening based on exponential maps. Eng. Comput. **24**(6), 608–635 (2007)
28. Rezaiee-Pajand, M., Nasirai, C.: On the integration schemes for Drucker-Prager's elasto-plastic models based on exponential maps. Int. J. Numer. Methods Eng. **74**, 799–826 (2008)
29. Rezaiee-Pajand, M., Nasirai, C., Sharifian, M.: Application of exponential-based methods in integrating the constitutive equations with multicomponent kinematic hardening. J. Eng. Mech. ASCE **136**(12), 1502–1518 (2010)
30. Rezaiee-Pajand, M., Sharifian, M., Sharifian, M.: Accurate and approximate integrations of Drucker-Prager Plasticity with linear isotropic and kinematic hardening. Eur. J. Mech. A Solids **30**, 345–361 (2011)
31. Rezaiee-Pajand, M., Nasirai, C., Sharifian, M.: Integration of nonlinear mixed hardening models. Multidiscip. Model. Mater. Struct. **7**(3), 266–305 (2011)
32. Ortiz, M., Simo, J.C.: An analysis of a new class of integration algorithms for elasto-plastic constitutive relations. Int. J. Numer. Methods Eng. **23**, 353–366 (1986)
33. Genna, F., Pandolfi, A.: Accurate numerical integration of Drucker-Prager's constitutive equations. Meccanica **29**, 239–260 (1994)
34. Hopperstad, O.S., Remseth, S.: A return mapping algorithm for a class of cyclic plasticity models. Int. J. Numer. Methods Eng. **38**, 549–564 (1995)
35. Kobayashi, M., Ohno, N.: Implementation of cyclic plasticity models based on a general form of kinematic hardening. Int. J. Numer. Methods Eng. **53**, 2217–2238 (2002)
36. Kobayashi, M., Mukai, M., Takahashi, M., Ohno, N., Kawakami, T., Ishikawa, T.: Implicit integration and consistent tangent modulus of a time-dependent non-unified constitutive model. Int. J. Numer. Methods Eng. **58**, 1523–1543 (2003)
37. Kang, G.: Finite element implementation of viscoplastic constitutive model with strain-range-dependent cyclic hardening. Commun. Numer. Methods Eng. **22**, 137–153 (2006)
38. Clausen, J., Damkilde, L., Anderson, L.: Efficient return algorithms for associated plasticity with multiple yield planes. Int. J. Numer. Methods Eng. **66**, 1036–1059 (2006)
39. Kan, Q.H., Kang, G., Zhang, J.: A unified visco-plastic constitutive model for uniaxial time-dependent ratchetting and its finite element implementation. Theor. Appl. Fract. Mech. **47**, 133–144 (2007)
40. Coombs, W.M., Crouch, R.S., Augarde, C.E.: Reuleaux plasticity: analytical backward Euler stress integration and consistent tangent. Comput. Methods Appl. Mech. Eng. **199**, 1733–1743 (2010)
41. Drucker, D.C., Prager, W.: Soil mechanics and plastic analysis or limit design. Quart. Appl. Math. **10**, 157–165 (1952)
42. Golub, G.H., Van Loan, C.F.: Matrix Computation. Johns Hopkins University Press, Baltimore, MD (1983)
43. Dormand, J.R., Prince, P.J.: A family of embedded Runge-Kutta formulae. J. Comput. Appl. Math. **6**(1), 19–26 (1980)
44. Arregui, I.L., Alfredsson, B.: Elastic-plastic characterization of a high strength bainitic roller bearing steel—experiments and modeling. Int. J. Mech. Sci. **52**, 1254–1268 (2010)